Loss of FBXO11 function establishes a stem cell program in acute myeloid leukemia through dysregulation of the mitochondrial protease LONP1

Angela Ya-Chi Mo[1,2], Hayle Kincross[1], Xuan Wang[1], Linda Ya-Ting Chang[1], Gerben Duns[1], Harwood Kwan[1], Tammy Lau[1], T. Roderick Docking[1], Jessica Tran[1], Shane Colborne[1], Se-Wing Grace Cheng[1], Shujun Huang[1], Nadia Gharaee[1], Elijah Willie[1], Jihong Jiang[1], Jeremy Parker[1], Joshua Bridgers[1], Davis Wood[3], Ramon Klein Geltink[2], Gregg B. Morin[1,4], Aly Karsan*[1,2]

[1]Michael Smith Genome Sciences Centre, BC Cancer, Vancouver, British Columbia, Canada.
[2]Department of Pathology and Laboratory Medicine, University of British Columbia, Vancouver, British Columbia, Canada.
[3]Centre for Comparative Medicine, University of British Columbia, Vancouver, British Columbia, Canada.
[4]Department of Medical Genetics, University of British Columbia, Vancouver, British Columbia, Canada.

* Corresponding Author: Aly Karsan, BC Cancer Research Institute
675 West 10th Avenue, Vancouver, British Columbia V5Z 1L3, Canada
Phone: 604.675.8034; e-mail: akarsan@bcgsc.ca

The authors declare that no conflict of interest exists

ABSTRACT

Acute myeloid leukemia (AML) is an aggressive cancer with very poor outcomes. Analysis of sequencing data from 1,627 unique AML patients revealed frequent mutations in ubiquitin ligase family genes. Loss of function of the Skp1/Cul1/Fbox (SCF) E3 ubiquitin ligase complex genes are found in ~8% of AML patients including recurrent mutations in *FBXO11*. *FBXO11* is the most significantly downregulated gene of the SCF complex in AML samples. Depletion of *Fbxo11* promotes myeloid-biased stem cell maintenance and cooperates with *AML1-ETO* and mutant *KRAS* to generate serially transplantable mouse and human AML in *in vivo* models. FBXO11 mediates K63-linked polyubiquitination of the LONP1 mitochondrial protease, and loss of *FBXO11* impairs LONP1 activity thereby reducing mitochondrial membrane potential, imparting stem cell properties and driving leukemogenesis. Our findings suggest that loss of FBXO11 function primes HSPC for myeloid-biased self-renewal through attenuation of LONP1-mediated regulation of mitochondrial function.

MAIN

Despite the introduction of new targeted therapies for acute myeloid leukemia (AML), outcomes remain dismal with 5-year survival being <35% overall, and around 10% in those over 60 years old[1]. Various sequencing studies have generated molecular classification systems for AML[2,3]. Nevertheless, in a large targeted sequencing study comprising 1,540 AML patients, which established 11 distinct molecular subclasses of AML based on cytogenetic abnormalities and driver mutations, at least 11% of the patients could not be classified into a specific group[3]. Analyses of gene expression studies have suggested that additional genetic, epigenetic and/or clinical parameters play a role in refining genetic classification[2,4].

Disruption of the ubiquitin pathway plays an important role in cancer development, as suggested by recurrent genetic aberrations affecting E3 ligases and deubiquitinases in multiple cancers[5–8]. Ubiquitination plays a crucial role in the development and function of normal hematopoietic stem and progenitor cells (HSPC) and leukemic stem cells (LSC)[9–13], but ubiquitin gene mutations do not currently constitute a molecular subclass in AML. Further, although the presence of a ubiquitin pathway mutation has generally been extrapolated to mean that the ubiquitin-proteasome system is defective[8,14,15], results of clinical trials with these inhibitors are conflicting, and suggest that ubiquitination functions independent of proteasome-mediated degradation may play an important role in AML[16].

A major issue in molecular characterization of AML is that it is difficult to identify subclasses that are comprised of rare mutations in many different genes across a molecular subclass. We found recurrent somatic mutations affecting multiple components of ubiquitinating enzyme complexes in the AML-Personalized Medicine Project (AML PMP) cohort[2], and confirmed these findings in the Beat AML, TCGA AML, and TARGET AML datasets[17–20]. Using an approach combining mutation analyses and gene expression changes, we identified diminished FBXO11 function – a member of the SKP-CUL-FBox E3 ligase family – to be a key aberration imparting LSC function in a subset of AMLs. Loss of *FBXO11* function was evidenced by truncating mutations or copy number loss, and reduced gene expression in AML compared to normal HSPC. Our analyses show that *FBXO11* depletion cooperates with other mutations to induce myeloid malignancy in mouse and human xenograft models. *FBXO11* depletion induces a myeloid-biased quiescent stem cell phenotype by regulating mitochondrial metabolism through K63-linked ubiquitination of the mitochondrial protease, LONP1.

RESULTS

Ubiquitin pathway mutations are frequent and mutually exclusive in AML cells

We analyzed RNA-seq data from the AML PMP dataset[2] to identify novel recurrent mutation classes that contribute to the initiation or maintenance of AML. In addition to single nucleotide variants (SNVs) and insertion and/or deletion mutants (indels) in previously described molecular subclasses of AML, we identified SNVs and indels in ubiquitin pathway genes in 11.4% (16/140) of the AML PMP cohort (Supplementary Fig. 1, Supplementary Table 1)[3,21]. Extending the cohort to include AML PMP, TCGA, Beat AML, and TARGET pediatric AML datasets for a total of 1,627 AML patients revealed ubiquitin pathway gene mutations in 163 patients (10%) (Fig. 1a, Supplementary Table 1). The vast majority of AMLs with ubiquitin pathway system mutations only had one mutation, consistent with mutual exclusivity (Fig. 1a), and suggesting a potential common functional effect of these mutations. Loss-of-function mutations including truncating mutations and copy number loss (based on karyotype in all cases and microarray data) of the *FBXO11* gene and other members of the Skp1-Cul1-Fbox (SCF) E3 ubiquitin ligase complex were identified in 8% (123/1627) of AML patients (Supplementary Fig. 1, Fig. 1a). Although there is evidence that deregulated ubiquitination plays a role in leukemogenesis[8,22], the current findings implicate ubiquitin pathway mutations as being an independent and distinct class of AML mutations (Fig. 1a).

Haplodeficiency of *FBXO11* promotes the maintenance of primitive cells with myeloid bias

To understand the implications of aberrant ubiquitination, we focused on the recurrently mutated *FBXO11* gene, which encodes the substrate-recognition component of the SCF^{FBXO11} E3 ubiquitin ligase complex. *FBXO11* variants occur in 1.8% of non-AML cancers in the TCGA dataset (Supplementary Fig. 2a, Supplementary Table 3). Of the 11 patients with *FBXO11* mutations, 2 patients had a truncating or frame-shift mutation and 7 patients had a single copy deletion (Supplementary Fig. 2b), suggesting haploinsufficiency of *FBXO11* in AML. Consistent with loss-of-function mutations, AML samples with *FBXO11* mutations or deletions had lower *FBXO11* transcript expression than wild-type cases (Supplementary Fig. 2c). To determine whether *FBXO11* expression was regulated in AML independent of genomic variants, we compared transcript expression of SCF genes in normal $CD34^+$ HSPC and in AML cells. Of all SCF genes, *FBXO11* was the most significantly downregulated in AML samples compared to normal $CD34^+$ HSPC (Fig. 1B and C, Supplementary Table 2). Accordingly, FBXO11

protein expression was less than 10% of the level expressed in the K562 cell line in 5/7 of the myeloid cell lines tested (Supplementary Fig. 2d).

To determine the effects of *FBXO11* depletion on human hematopoiesis, we analyzed RNA expression of human cord blood-derived $CD34^+$ HSPC lentivirally transduced with a short-hairpin (sh)RNA targeting *FBXO11 (*sh*FBXO11*) or a non-targeting shRNA (shCTR). Depletion of *FBXO11* in human $CD34^+$ HSPC resulted in enrichment of HSC and LSC signatures and diminishment of progenitor cell and heme metabolism signatures compared to control (Fig. 2a, Supplementary Fig. 3a). Liquid culture of $CD34^+$ HSPC resulted in increased $CD34^+$ cell proportions with *FBXO11* knockdown compared to control (Fig. 2b). As absolute cell numbers of $CD34^+$ cells were lower in sh*FBXO11*- than shCTR-transduced cells (Fig. 2b), we postulated that *FBXO11* knockdown promoted quiescence as seen in dormant long-term stem cells. Cell cycle analysis confirmed that *FBXO11* depletion increased the G_0 fraction in the $CD34^+$ population (Fig. 2c). Interestingly, although increased in the bulk cultured population of sh*FBXO11* cells, cell death was attenuated in the $CD34^+$ fraction (Supplementary Fig. 3b), suggesting a protective effect of *FBXO11* depletion in HSPC.

To verify a role for *FBXO11* depletion in supporting a stem cell phenotype, we examined the immunophenotype of cultured primary $CD34^+$ HSPC exhibiting functional short-term and long-term stem cell ($CD45RA^-$) or progenitor cell ($CD90^-CD45RA^-$) markers[23]. *FBXO11* depletion increased the stem cell-like population, at the expense of the progenitor-like population (Fig. 2d, Supplementary Fig. 3c). In this culture system, all $CD34^+$ cellular subpopulations showed an increase in the G_0 fraction, consistent with *FBXO11* depletion inducing quiescence as found in the total $CD34^+$ population (Fig. 2c, Supplementary Fig. 3d).

To examine cell output in *FBXO11*-depleted cells, we cultured $CD34^+$ HSPC following knockdown of *FBXO11*. Following 7 days in liquid culture *FBXO11*-depleted cells displayed myeloid-biased output with expansion of $CD15^+$ myeloid cells, but reduction in erythroid (CD71/CD235a) and megakaryocytic (CD41/CD61) populations compared to control (Fig. 2e). *FBXO11* knockdown resulted in reduced primary colony forming cell (CFC) counts (Fig. 2f), with increased clonogenic activity on secondary replating (Fig. 2g), consistent with activation of a quiescent HSPC population. In primary CFC assays, there was significant reduction of erythroid colonies in keeping with the reduced heme metabolism gene expression signature and reduced erythroid differentiation in liquid culture (Fig. 2a, e), and consistent with a previous report demonstrating a role for FBXO11 in erythropoiesis[24]. Together these results

suggest that *FBXO11* depletion in human CD34$^+$ cells results in a quiescent myeloid-biased primitive hematopoietic population with stem cell characteristics.

***Fbxo11* depletion cooperates with *AML1-ETO* to generate serially transplantable mouse leukemia**

One sample with an *FBXO11* mutation had a cooccurring *AML1-ETO* (*RUNX1-RUNX1T1*) fusion (Fig. 1a). Since expression of the *AML1-ETO* fusion gene is common in leukemia but not sufficient in isolation to generate murine leukemia[25], we examined whether *FBXO11* depletion would cooperate with *AML1-ETO* to drive leukemogenesis[26]. Mouse bone marrow HSPC were co-transduced with human *AML1-ETO* and sh*Fbxo11*, and transplanted into lethally irradiated mice. Marrow HSPC expressing *AML1-ETO* with control shRNA (shLuc), sh*Fbxo11* with empty vector (MIG), or shLuc with MIG were included as controls (Supplementary Fig. 4a). Mice reconstituted with HSPC expressing sh*Fbxo11* with *AML1-ETO* developed myeloid leukemia, with reduced leukemia-free survival compared to mice reconstituted with HSPC expressing *AML1-ETO* alone (median survival of 164 vs 280 days, respectively) (Fig. 3a).

At endpoint, *AML1-ETO*/sh*Fbxo11* transplanted mice exhibited leukocytosis, anemia, thrombocytopenia and splenomegaly (Supplementary Fig. 4b) with significant expansion of the Lin$^-$Kit$^+$ (LK) myeloid progenitor population in the peripheral blood (Fig. 3b), and increased leukemic blasts in the bone marrow and peripheral blood (Fig. 3c, Supplementary Fig. 4c). Further, *AML1-ETO*/sh*Fbxo11* mice had significant expansion of an immunophenotypic long-term reconstituting hematopoietic stem cell (LT-HSC)-like population compared to the three other control groups (Fig. 3d, Supplementary Fig. 5). Serial transplantation of bone marrow harvested from *AML1-ETO*/sh*Fbxo11* mice resulted in more aggressive secondary leukemias, consistent with expansion of an LSC population (Fig. 3e). Thus, while neither sh*FBXO11* nor *AML1-ETO* alone was sufficient to generate acute leukemia, the combination of *AML1-ETO* with depletion of *Fbxo11* initiated and maintained murine myeloid leukemias.

***FBXO11* depletion cooperates with *AML1-ETO* and *KRAS*^{G12D} to generate human myeloid leukemia**

Previous studies have shown that the combination of *AML1-ETO* with mutant *RAS* is not sufficient to transform human CD34$^+$ cells, and to-date there is no known combination of mutants with *AML1-ETO* that results in human leukemia[27]. As ubiquitin pathway mutations cooccur with *RAS* mutations (Fig. 1a, Supplementary Fig. 6), we asked whether the combination of *AML1-ETO*, activated KRAS and *FBXO11* depletion could initiate human leukemia. We transduced CD34$^+$ cells with combinations of these variants, and expanded the cells in long-term culture followed by

xenotransplantation into NOD.*Rag1*$^{-/-}$;*γc*^{null} (NRG) mice expressing human *IL3*, human *GMCSF*, and human *SCF* (NRG-3GS). CD34^{+} cells were transduced with empty vector (EV), *FBXO11* shRNA (F), K *KRAS*^{G12D} (K), AML1-ETO (A), F+A (FA), F+K (FK), K+A (KA), or all three (FKA), and flow-sorted for the co-expressed fluorescent markers (Fig. 4a).

Following long-term co-culture, *FBXO11* knockdown resulted in reduced cell numbers, but significant enrichment of the proportion of CD34^{+} cells when combined with A or KA relative to corresponding controls (Fig. 4b, Supplementary Fig. 7a). Only the combination of all three genetic perturbations (FKA) permitted progenitor readout in CFC assays (Supplementary Fig. 7b). Xenotransplantation of EV, KA, and FKA cells into NRG-3GS mice resulted in significantly reduced overall survival in FKA mice (Fig. 4c). However, of the mice that survived, those with transplanted FKA cells had significantly longer and higher human hematopoietic reconstitution compared to KA- and EV-transplanted mice, suggesting that *FBXO11* knockdown improves long-term *in vivo* repopulating ability of human HSPC (Fig. 4d, Supplementary Fig 8).

Morphological examination at endpoint revealed blast cells in the bone marrow, and leptomeningeal infiltration with primitive myeloid cells, consistent with myeloid leukemia (Fig. 4e, Supplementary Fig. 9a, b). FKA mice had significantly increased human hematopoietic cell reconstitution in the spleen and bone marrow, >98% of which were CD33^{+} myeloid cells (Fig. 4f-h, Supplementary Fig. 10a). FKA-transplanted mice also had greater numbers of CD34^{+} bone marrow cells at endpoint (Fig. 4i, Supplementary Fig. 10b). Human CD34^{+} cell output post-transplant per initial CD34^{+} cell placed in long-term culture revealed ~6,000-fold expansion of FKA HSPC, while KA HSPC did not result in CD34^{+} cell expansion (Supplementary Table 4, Supplementary Fig. 10c).

Serial marrow transplantation resulted in enhanced reconstitution of human hematopoietic populations with FKA cells compared to controls, indicating maintenance or expansion of self-renewing hematopoietic cells (Fig. 4j). Taken together, these results demonstrate that *FBXO11* depletion improves long-term *in vivo* human cell reconstitution, consistent with induction of a myeloid-skewed, long-term self-renewing stem cell state that cooperates with *KRAS*^{G12D} and *AML1-ETO* to generate myeloid malignancy.

FBXO11-mediated ubiquitination positively regulates LONP1 mitochondrial function.

To identify substrates of the SCF^{FBXO11} complex, we immunoprecipitated FLAG-tagged FBXO11 (FLAG-*FBXO11*) in the presence or absence of endonuclease treatment, and identified 5 common

coimmunoprecipitating proteins using tandem mass spectrometry, including components of the SCF^{FBXO11} complex, SKP1, CUL1 and FBXO11 (Fig. 5a). Additional proteins included the mitochondrial protease, LONP1, and the transcriptional repressor THAP5 (Fig. 5a, Supplementary Fig. 11). FBXO11 interaction with LONP1 was confirmed by reciprocal co-immunoprecipitation and western blotting (Supplementary Fig. 12), but we were not able to confirm FBXO11 interaction with THAP5. Dysregulation of LONP1 has been associated with colon cancer and melanoma, but has not been studied in the context of AML[28–30].

Surprisingly, LONP1 protein abundance was not affected by *FBXO11* depletion or overexpression, suggesting that LONP1 is not targeted by SCF^{FBXO11} for proteasomal degradation (Fig. 5b). If FBXO11 acts to activate rather than degrade LONP1, depletion of LONP1 should recapitulate the functional effects of FBXO11 depletion. Indeed, *LONP1* depletion had a similar effect as *FBXO11* depletion on primary $CD34^+$ HSPC differentiation, causing a reduction in the $CD41^+CD61^+$ megakaryocytic and $CD71^+CD235a^+$ erythroid populations, and an increase in the $CD14^+$ and $CD15^+$ myeloid populations (Fig. 5c), supporting a model of FBXO11 activating LONP1.

LONP1 is a mitochondrial protease and chaperone protein that has been reported to target misfolded subunits of ETC complex II and complex V for degradation[31]. Consequently, *LONP1* loss reduces oxygen consumption rate and mitochondrial membrane potential (MMP)[30,31]. LT-HSCs and $CD34^+$ HSPC with greater reconstitution potential have reduced MMP, and the disruption of MMP promotes self-renewal in HSCs[32–34]. This is consistent with our data showing that *FBXO11* depletion promotes a stemness phenotype. *LONP1* knockdown reduced MMP, as did *FBXO11* knockdown in 2 myeloid cell lines as well as primary $CD34^+$ HSPC (Fig. 5d). Lower MMP was not accompanied by a reduction in mitochondrial mass, suggesting a defect in the electron transport chain (ETC), which is responsible for maintaining MMP (Supplementary Fig. 13). Concordant with this hypothesis, a lower basal respiration rate was observed in *FBXO11*-KO cells compared to *FBXO11*-KO cells reconstituted with wild-type (WT) FLAG-FBXO11 (Supplementary Fig. 14). In contrast, overexpression of WT FLAG-*FBXO11*, but not an F-box domain mutant (ΔFbox-FBXO11) which does not interact with LONP1, increased MMP as expected (Fig. 5e, Supplementary Fig. 15). Thus, FBXO11 interaction with its target protein, LONP1, is necessary for regulating mitochondrial function. To address whether *LONP1* expression is required for FBXO11 functional effects, we combined *LONP1* knockdown with enforced FLAG-*FBXO11* expression. The increase in MMP from FLAG-*FBXO11* expression was blocked by *LONP1* knockdown, indicating that

LONP1 is required for mitochondrial regulation by FBXO11 and that LONP1 functions downstream of FBXO11 (Fig. 5f).

We next considered potential activating functions of SCF^{FBXO11} as an E3 ubiquitin ligase complex, or an E3 NEDD8 ligase complex[35,36]. Although K63-linked polyubiquitination activity has not previously been reported for this complex, we immunoprecipitated LONP1 and blotted for K63-linked polyubiquitination and NEDD8. FLAG-*FBXO11* expression increased both K63-linked polyubiquitination and neddylation of LONP1 (Fig. 5g, h), consistent with the potential for FBXO11 having an activating effect on LONP1, mediated through either one or both of these modifications.

In order to determine whether ubiquitination or neddylation is responsible for LONP1 activation by FBXO11, K562 cells were lentivirally transduced to express FLAG-*FBXO11* to increase basal MMP levels, and then treated with ubiquitin activating enzyme or NEDD8-activating enzyme inhibitors to determine if either mimicked the effect of *FBXO11* depletion. Only treatment with ubiquitin- but not NEDD8-activating enzyme inhibitors resulted in reduced MMP as observed with *FBXO11* knockdown (Fig. 5i). As would be predicted, proteasome inhibitors also did not reduce FBXO11-mediated MMP elevation, implicating FBXO11-mediated activating ubiquitination of LONP1, rather than proteasomal degradation in regulating its mitochondrial function (Fig. 5j).

Transcriptomic trends are consistent with a model of FBXO11 activating LONP1 to regulate stem cell maintenance.

As an alternate approach to confirm that FBXO11 regulates LONP1 function, we performed RNA-seq on primary $CD34^+$ HSPC expressing combinations of shRNAs targeting *FBXO11* or *LONP1* alone, or combined with enforced *LONP1* or FLAG-*FBXO11* expression (Supplementary Fig. 16). Analysis of the samples based on Euclidean distances clustered *LONP1* overexpressing samples with control conditions (Fig. 6a), suggesting that overexpression of LONP1 is not sufficient for increased activity, and likely requires activation, potentially by FBXO11. Similarly, *FBXO11* knockdown samples (shFBXO11_9) also clustered closely with samples with *FBXO11* knockdown and *LONP1* overexpression (shFBXO11_LONP1), suggesting that LONP1 overexpression cannot reverse the phenotype generated by depletion of *FBXO11*. Principal component analysis (PCA) confirmed the findings that LONP1 overexpression was not sufficient to alter gene expression, but knockdown of LONP1 inhibited the transcriptional response evoked by FBXO11 overexpression (Supplementary Fig. 17).

Given that *FBXO11* depletion results in a stem cell phenotype, and *FBXO11* and *LONP1* depletion result in reduced mitochondrial activity, we performed Gene Set Enrichment Analysis (GSEA) to confirm that the HSC and mitochondrial functional effects initiated by *FBXO11* depletion are dependent on loss of LONP1 function. Both *FBXO11* and *LONP1* knockdown positively enriched for HSC/LSC gene sets (Fig. 6b). FLAG-*FBXO11* expression had the opposite effect with reduced expression of genes in the HSC-LSC gene set, while constitutive *LONP1* expression had a negligible effect. *LONP1* depletion blocked the effect of FLAG-*FBXO11* overexpression, indicating that FBXO11-mediated loss of stemness is mediated by LONP1. These results further support the role of LONP1 as a mediator of FBXO11-driven loss of stem cell characteristics. Similar trends were present in HSC and mitochondrial respiratory chain defect gene sets, which were enriched in upregulated genes with *FBXO11* and *LONP1* knockdown and overrepresented in the downregulated genes with constitutive *FBXO11* expression, while *LONP1* knockdown reversed or blocked the effect of *FBXO11* expression (Fig. 6c). Accordingly, the opposite trend was observed in a progenitor gene set, which was overrepresented in the downregulated genes when *FBXO11* or *LONP1* was knocked down, and enriched in the upregulated genes with *FBXO11* overexpression (Fig. 6c). Consistent with transmitting FBXO11 functions, *LONP1* knockdown blocked the loss of a stem cell signature and mitochondrial effects of enforced *FBXO11* expression (Fig. 6c). These gene expression patterns support a model of *FBXO11* depletion regulating mitochondrial function and stem cell maintenance through reduced LONP1 function.

Next, we examined whether *FBXO11* and *LONP1* knockdown enriched for a stem cell transcriptomic state with myeloid bias, as shown based on results from previous experiments. Genes that were upregulated with the knockdown of *FBXO11* and *LONP1* shared similar transcriptomic profiles, with enrichment in genes associated with HSC and myeloid cell populations including common myeloid progenitors (CMP), granulocyte-monocyte progenitors (GMP), myelocytes, and myeloid dendritic cells (mDC) (Fig. 6d). Aligning with these trends, genes downregulated with FLAG-*FBXO11* expression were strongly enriched in HSC, CMP, and GMP associated genes, but when combined with *LONP1* knockdown, this effect was attenuated and the megakaryocyte-erythroid progenitor state was enriched (Fig. 6d, e). The latter aligns with the loss of megakaryocytic and erythroid differentiation with *LONP1* depletion that we observed in HSPC, again demonstrating that *LONP1* expression is required for FBXO11 functional effects. We also noted that the transcriptomic profile of cells with *FBXO11* depletion combined with *LONP1* overexpression highly resembled cells with *FBXO11* depletion alone, further supporting a model of LONP1 function that is dependent on *FBXO11*-mediated regulation (Fig. 6f).

DISCUSSION

In this work we highlight ubiquitin pathway mutations as a novel class of AML mutations. We implicate *FBXO11* depletion in leukemogenesis, and identify a novel connection between ubiquitination and mitochondrial function through FBXO11-mediated regulation of the mitochondrial protease and chaperone, LONP1, independent of the proteasome system. Consistent with previously characterized activating effects of K63-linked polyubiquitination of target proteins, our data suggest that FBXO11 modification of LONP1 promotes LONP1 mitochondrial function resulting in an increase in MMP. Our results further suggest that FBXO11 ubiquitination of LONP1 is required to activate LONP1 function. This activating effect is in contrast to the few other FBXO11 targets previously reported. For instance, SCF^{FBXO11} has been shown to target BCL6, CRL4, and Snail family transcription factors for ubiquitination and subsequent proteasomal degradation[37–39]. SCF^{FBXO11}-mediated neddylation of p53 also inhibits p53 transcriptional activity[35]. Our findings provide an explanation as to why *LONP1* was not detected in a screen for identifying mitochondrial contributors to leukemogenesis, as the readout in that study was reduced leukemia cell viability with target gene knockdown[40]. In our model, it is reduced LONP1 function due to *FBXO11* depletion, not LONP1 activation, that is responsible for leukemogenesis.

The RNA-seq expression data support FBXO11 as an upstream regulator of LONP1 and solidify the mitochondrial defect link between *FBXO11* and *LONP1* depletion. The mitochondrial respiratory chain defect geneset expression trends are consistent with the reduced MMP characteristic of functional stem cells we observed with *FBXO11* and *LONP1* depletion. Of interest, the reduction in erythroid differentiation resulting from *LONP1* depletion, which mimicked the effects of *FBXO11* depletion and is also reflected in our transcriptomic data is supported by previous reports on the role of LONP1 in heme biosynthesis[41].

Loss of ETC function can result from the accumulation of misfolded ETC proteins shown to occur with *LONP1* loss, or from loss of LONP1 chaperone activity required for proper folding of some ETC proteins[31,42]. We found that both *FBXO11* and *LONP1* depletion reduced MMP, and that FBXO11 acts through regulation of LONP1. LT-HSCs and $CD34^+$ cells that have greater reconstitution potential are both characterized by low MMP[32–34]. Disruption of MMP also promotes self-renewal in HSCs, indicating that low MMP is essential for maintaining an HSC state[34]. Additionally, while *FBXO11* depletion has previously been shown to impart apoptotic effects, our work shows that this is not true for primitive HSPC. Rather, *FBXO11*-depleted HSPC are protected from apoptosis and remain in G_0 of the cell cycle.

These findings are also consistent with the stem cell characteristics we observed with *FBXO11* depletion, both functionally, and at the transcriptional level.

While mitochondrial metabolism and function in stem cells have recently been a focus in stem cell research, there is no consensus on how exactly reduced mitochondrial function promotes a stem cell state or contributes to leukemogenesis. Metabolic changes and products of metabolic pathways have been shown to impact nuclear transcription as well as chromatin and epigenetic remodeling, particularly in cancers[43,44]. In fact, changes in MMP have previously been shown to affect nuclear gene expression in macrophages, suggesting one mechanism for how reduced mitochondrial function might promote a stem cell state[45].

In this work, we suggest that mutations of ubiquitin pathway genes may represent a novel molecular subclass in AML. Further, we demonstrate the leukemogenic effects of *FBXO11* loss. We draw a novel connection between the ubiquitin pathway and the mitochondrial protease system. In particular, we show that LONP1 is a target that is activated, rather than degraded following FBXO11-mediated ubiquitination, and this acts as a regulator of hematopoiesis. Importantly, this work suggests that altered gene expression independent of genetic variants may implicate ubiquitin system gene defects in a much wider cohort of AML patients.

METHODS AND MATERIALS

Mutation calling for oncoprint inclusion

Patient mutations were determined pathogenic and included in the oncoprint if they had a REVEL score > 0.250 and CADD score > 10.5. Germline variants were excluded. Hugo Gene Nomenclature Committee (HGNC) gene data was used to generate a list of ubiquitination genes to query, and the list was manually filtered to retain genes functionally relevant to the UPS. For determining the REVEL score threshold of 0.25 for pathogenicity, data for pathogenic solid tumor variants were obtained from *Cheng et al* (Memorial Sloan Kettering-Integrated Mutation Profiling of Actionable Cancer Targets (MSK-IMPACT))[46], and variants that were reported less than five times in the Catalogue of Somatic Mutations in Cancer (COSMIC) were excluded. Pathogenic variants associated with human hematological cancers were obtained from *Jaiswal et al*[47], and variants that were reported less than 5 times in COSMIC were excluded.

Odds ratios calculations

Odds ratios were calculated as "odds of a mutation occurring in a sample with a UPS mutation" vs "odds of a mutation occurring in a sample without UPS mutations".

Odd ratio for mutations in gene X=

$$\frac{\text{\# patients with mutation in X and at least 1 UPS mutation}}{\text{\# patients with at least 1 UPS mutation}} \Big/ \frac{\text{\# patients with mutation in X and no UPS mutations}}{\text{\# of patients with no UPS mutations}}$$

Isolation of human HSPCs

Human HSPC isolation was performed by the Stem Cell assay core at BC Cancer Research Institute. Anonymized normal human cord blood samples were obtained with informed consent from normal full-term Cesarean section deliveries in accordance with procedures approved by the Research Ethics Board of the University of British Columbia and samples from a single day pooled for further processing. $CD34^+$ HSPCs were obtained at >95% purity from pooled collections using a two-step Rosette-Sep/EasySep human CD34-positive selection kit (STEMCELL Technologies) according to the manufacturer's protocols and/or FACS sorting. CB cells were thawed by dropwise addition into HBSS + 10% fetal bovine serum (FBS) supplemented with DNase (100 µg/mL final concentration). $CD34^+$ HSPCs were then seeded into 96-well round bottom plates (cell density at 100,000 (100k) cells/100 µL) and prestimulated in StemSpanTM SFEM (Stem Cell Technologies #09650) supplemented with StemSpan™ CC100 (Stem Cell Technologies #02690), 750 nM SR1 (Stem Cell Technologies #72344) and 35 nM UM171(Stem Cell Technologies #72912) overnight.

shRNA constructs and CRISPR clones

K562 control and *FBXO11* knockout CRISPR clones were generated by Dr. Gerben Duns. Guide RNAs (gRNAs) were cloned into the pSpCas9n(BB)-2A-GFP (PX461) plasmid (Addgene #48140) and delivered to parental K562 cells by Amaxa nucleofection using the Amaxa Cell line nucleofector kit V (Lonza VCA-1003). GFP+ transfected cells were single-cell sorted into 96-well plates, expanded. *FBXO11* targeting was confirmed by Sanger sequencing, and FBXO11 depletion was confirmed by western blot. shRNAs used are in the pLKO.1 vector, from the MISSION library, and received from the UBC Centre for High-Throughput Biology, and GFP or mCherry was inserted in place of the puromycin resistance marker. gRNA and shRNA information are listed below. More information for gRNA and shRNA targeting can be found in Appendix Figures A.3 and A.4.

***FBXO11* CRISPR gRNAs**

gRNA sequence: AACCACTGTAGGGTTAGCATAGG

Target exon: Exon 12/23 (antisense, positive strand)

Mouse shRNA

TRC clone ID: TRCN0000238633

Target: NM_001081034.1 at 1143-1164

Target sequence: AGTCAACTGCAGCCCTATTAT

Human shRNAs

shCTR

Target sequence: CCTAAGGTTAAGTCGCCCTCGC

sh*FBXO11* #9

TRC Clone ID: TRCN0000004303

Target exon: Exon16/23 (isoform 4 NM_001190274.2)

Target sequence: GAGTGCTAGAAGACAATGATA

sh*FBXO11* #10

TRC Clone ID: TRCN0000004304

Target exon: Exon 5/23 (of isoform 4 NM_001190274.2)

Target sequence: GAGAGTTTCCAGCAGTTGTAT

shLONP1 #1

TRCN0000046793, Exon 11/18 (isoform 1 NM_004793.4)

Target sequence: CCAGTGTTTGAAGAAGACCAA

shLONP1 #3

TRCN0000046797 Exon 2/18 (isoform 1 NM_004793.4)

Target sequence: CCAGCCTTATGTCGGCGTCTT

Retroviral constructs

Mouse shRNAs were cloned into the pSIREN-RetroQ plasmid (Addgene #73666). The *AML1-ETO* overexpression construct was purchased from Addgene (#12431).

Lentiviral constructs and transduction

High-titre lentiviral supernatants were produced by transient transfection of 293T/17 cells with second-generation packaging/envelope vectors pRRE (Addgene #12251), pREV (Addgene #115989), and pMD2.g (Addgene #12259) using CalPhosTM mammalian transfection kit (Clontech #631312) and incubated for 16 hours, followed by ultracentrifuge concentration (25,000 rpm for 90 min at 4°C; Beckman SW32Ti rotor).

$CD34^+$ HSPCs were transduced in 96-well plates (Thermo ScientificTM #12-565-65) with concentrated lentivirus. After 6 hours of incubation, cells were washed once with PBS and transferred to culture medium (StemSpanTM SFEM with StemSpan™ CC100 to culture medium at a 1 in 100 dilution, 750 nM SR1 and 35nM UM171). Following 72-hour ex vivo culture, transduced cells were then isolated by sorting for reporter fluorophore expression from lentiviral constructs on a Fusion sorter (Becton Dickenson) using purity mode.

***Ex vivo* cord blood liquid culture for differentiation assay**

Transduced cells were sorted into 96-well plates at 10k cells/well into 100 µL in StemSpanTM SFEM supplemented with StemSpan™ CC100, 20 ng/mL recombinant human thrombopoietin (hTPO) (BioLegend #597402), DNase (100 µg/mL final concentration), and antibiotics (pencillin and

streptomycin). Cells were incubated in a humidified atmosphere at 37°C in room air supplemented with CO2 to achieve a final concentration of 5%.

Cell differentiation analysis

$CD34^+$ HSPCs were harvested from culture and washed with PBS with 2% FBS before staining with antibodies at the dilutions listed in Table 2.1 for 1 hour on ice. Cells were pelleted at 300 x g for 5 min, resuspended in PBS with 2% FBS and 1 µg/mL DAPI, and filtered before flow cytometry analysis.

Antibody target	Fluorochrome	Dilution	Clone	Vendor	Catalogue #
CD34	AF700	1:50	581	BD	561440
CD14	APC-Cy7	1:100	63D3	BioLegend	367108
CD11b	BV510	1:100	ICRF44	BioLegend	301334
CD41	PE	1:100	HIP8	BioLegend	303706
CD61	PE-Cy7	1:100	VI-PL2	BioLegend	336416
CD235a	BV711	1:100	HI264	BD Biosciences	740785
CD71	PerCP-Cy5.5	1:100	CY1G4	BioLegend	334114
CD33	BV510	1:100	WM53	BD	563257
CD15	BV786	1:100	HI98	BD	563838

Antibodies for mouse peripheral blood analysis

Antibody target	Fluorochrome	Dilution	Clone	Vendor	Catalogue #
c-Kit	BV650	1:100	2B8	BD	563399
CD45.2	APC-eFluor780	1:100	104	eBioscience	47-0454-82
CD3	PerCP-Cy5.5	1:300	17A2	BD	560527
CD19	APC	1:500	1D3	BD	561738
GR-1	PerCP-Cy5.5	1:2000	RB6-8C5	BD	561103
CD11b	APC	1:800	M1/70	BD	553312

Antibodies for mouse bone marrow analysis

Antibody target	Fluorochrome	Dilution	Clone	Vendor	Catalogue #
GR1	PerCP-Cy5.5	1:240	RB6-85C	BD	552093
Ter119	PerCP-Cy5.5	1:15	TER119	eBioscience	45-5921-82
B220	PerCP-Cy5.5	1:60	RA3-6B2	eBioscience	45-0452-80
CD3	PerCP-Cy5.5	1:30	172A	BD	560527
CD4	PerCP-Cy5.5	1:60	RM4-5	BD	550954
CD8a	PerCP-Cy5.5	1:60	53-6.7	BD	551162
IL7R	PerCP-Cy5.5	1:30	A7R34	eBioscience	45-1271-82
cKit	APC	1:10	2B8	eBioscience	17-11171-83
CD16/32	APC-Cy7	1:30	2.4G2	BD	560541
Sca1	PE-Cy7	1:15	D7	BD	558162
CD45.1	FITC	1:10	A20	eBioscience	A14732
Flk2/Flt3	PE-CF594	1:5	A2F10.1	BD	562537
CD34	Biotin	1:2.5	RAM34	eBioscience	13-0341-85
Streptavidin	BV650	1:30	-	BD	563855

Long-term initiating cell (LTC-IC)

Two-three days before cell sorting for long-term co-culture with MS5 feeder cells, frozen and X-ray irradiated feeder cells were thawed via dropwise addition into 9 mL DMEM with 15% FBS (15% DMEM) (Invitrogen, 12100-046). The cell mixture was spun down at 300 × g for 5 min and the supernatant was decanted. The cell pellet was then resuspended in 6 mL 15% DMEM (no antibiotics) and plated at 1 mL/dish in collagen-coated 35 mm dishes (collagen was neutralized with DMEM medium before cell plating). The feeder cells were incubated in a 37° C incubator overnight. The media was replaced with 2 mL fresh 15% DMEM medium the next day. On the day of $CD34^+$ HSPC cell sort, the media was removed and replaced sorted CB cells in 2.5 mL of LTC media (STEMCELL Technologies #05150) supplemented with 10 µM Hydrocortisone (STEMCELL Technologies #07904).

Weekly half-medium changes were performed by removing one half of the medium containing cells and replacing with freshly prepared H5100 with 10 µM hydrocortisone over the 40-day culture period.

Colony-forming cell (CFC) assay

For primary CFCs, 500 of sorted lentivirally transduced $CD34^+$ HSPCs were seeded into 1 mL of MethoCultTM H4434 Classic media (STEMCELL Technologies #04434) supplemented with StemSpan™

CC100 and antibiotics, and plated in 35mm CFC dishes (STEMCELL Technologies #27150). Cells were incubated for 10 days before colonies were counted.

For secondary CFCs, the media containing the cells were collected from the CFC dishes and transferred into 15mL tubes. PBS with 2% FBS was used to rinse the plates and pooled with the collected media. Cells were spun down at 300 x g for 5min, washed with PBS with 2% FBS. After cell counting, the cells were seeded into fresh CFC dishes in fresh MethoCultTM H4434 Classic media supplemented with StemSpan™ CC100 and antibiotics at 50k cells/mL in each plate. Colonies were counted after 10 days.

Mouse bone marrow transplants

C57BL/6J-c2J mice were lethally irradiated at 8.1 Gy and reconstituted with 5-fluoro-uracil-treated bone marrow cells obtained from Pep3B mice retrovirally transduced to express indicated constructs via tail vein injections. C56BL/6J-c2J mice were obtained from The Jackson Laboratory. Pep3B mice were bred in-house at the BC Cancer Research Centre.

Xenotransplantation

All experimental procedures were done in accordance with protocols approved by the University of British Columbia Animal Care Committee. NRG-3GS mice (NOD.Cg-*Rag1tm1Mom Il2rgtm1Wjl* Tg(CMV-IL3,CSF2,KITLG)1Eav/J)) were bred and maintained in the Animal Resource Centre of the British Columbia Cancer Research Centre under pathogen-free conditions.

Female NRG-3GS mice 8-15 weeks of age were sublethally irradiated with 850 cGy (cesium irradiation, medium dose rate) on the day of intrafemoral injection. 100k $CD34^+$ HSPCs harvested from LTC were injected per mouse. For transplant analysis of *ex vivo* cultured cells, bone marrow aspirates were performed every 6 weeks post-transplant and human chimerism was tracked by flow cytometry analysis (using a BD LSR Fortessa analyzer or BD FACSymphony) and analyzed with the following: APC-anti-CD45 2D1(1:50; Invitrogen 17-9459-42), APC/Cy7 anti-CD45 HI30 (1:50; BioLegend 304014), AF700-anti-CD34 (1:50; BD biosciences 561440), PE/Cy7-anti-CD33 (1:100; Thermo fisher 25-0338-42), PE/Cy7-anti-CD15 (1:100; BD biosciences 560827), BV650-anti-CD19 (1:100; BD biosciences 560827), SB600-anti-CD3(1:50; Invitrogen 83-0037-42), DAPI (1 µg/mL final concentration, Sigma-Aldrich D9542).
Bone marrow aspirates were performed on the non-injected femur (BM, weeks 6, 20, and 35 weeks post-transplant) or the injected femur (IF, weeks 12 and 27 weeks post-transplant) to determine human

cell chimerism. Engraftment is considered long term if detection threshold of >0.01% $CD45^+$ cells is exceeded at 20 weeks.

Transplanted mice were sacrificed at predefined, humane clinical morbidity endpoints. At endpoint, human chimerism in bone marrow (cells flushed from femurs, pelvis and tibias), spleen, and liver were tracked by flow cytometry analysis (using a BD LSR Fortessa analyzer or BD FACSymphony) and analyzed with the following: APC-anti-CD45 2D1(1:50; Invitrogen 17-9459-42), APC/Cy7 anti-CD45 HI30 (1:50; BioLegend 304014), AF700-anti-CD34 (1:50; BD biosciences 561440), PE -anti-CD33 (1:50; eBioscience 8012-0337-120), PE/Cy7-anti-CD15 (1:100; BD biosciences 560827), BV480-anti-CD14 (1:50; BD biosciences 566190), DAPI (1 µg/mL final concentration, Sigma-Aldrich D9542).

For secondary transplants, viably frozen bone marrow harvested at primary transplant endpoints were thawed and added drop-wise into 8mL thawing medium (PBS with 10% FBS and 100 µg/mL DNAse final concentration). Cells were spun down at 400 x g for 5 min to remove the supernatant. Cells were counted, and the total amount of harvested bone marrow for each EV and KA mice were transplanted into each sublethally irradiated recipient NRG-3GS by tail vein injection. Half of the harvested bone marrow from each donor FKA mouse was transplanted into each FKA recipient mouse. Secondary transplanted mice were monitored, processed, and analyzed following the procedures for primary transplants.

Calculating $CD34^+$ cell output for xenotransplants

The number of human $CD34^+$ cells generated per input $CD34^+$ cell after the LTC-IC and xenotransplant process is calculated based on the assumption that the ratio of the (**A**) number of $CD34^+$ cells harvested from the LTC to (**B**) the number of $CD34^+$ cells that were injected into the mice (**C**) X = the number of $CD34^+$ cells that would have been harvested at xenotransplant endpoint if the total amount of $CD34^+$ cells harvested from the LTC were injected into the mice to (**D**) the number of $CD34^+$ cells that were actually harvested from at xenotransplant endpoint. Since equal numbers (100k) of total cells harvested from LTC was injected into recipient mice for xenotransplantation, the number of $CD34^+$ transplanted varied between conditions.

To calculate the number of $CD34^+$ cell generated by the end of the experiment per $CD34^+$ cell inputted into the LTC-IC experiment, we divide “X” by the number of LTC-IC input $CD34^+$ cell, which is the same for each condition.

$$\frac{A}{B} = \frac{C}{D}$$

$$\frac{\#CD34^{+} \text{ cells at LTC harvest}}{\text{In vivo } CD34^{+} \text{ input cells injected}} = \frac{X}{\text{Average } \#CD34^{+} \text{ cells in BM at endpoint}}$$

RNAseq extraction and RNAseq

$CD34^{+}$ HSPCs were cultured for 24 hours in StemSpanTM SFEM supplemented with StemSpan™ CC100, 20 ng/mL recombinant hTPO, 750 nM SR1, 35 nM UM171, DNase (100 ug/mL final concentration), and antibiotics after sorting for lentivirally transduced cells as described above before pelleting at 300 x g for 5 min. Cell pellets were resuspended in TRIzolTM reagent (ThermoFisher #15596026). Total RNA was extracted according to manufacturer guidelines. For RNA precipitation, 5 µg glycogen (Roche #10901393001) was added per sample. 40 ng of RNQA per sample was submitted based on quantification by NanoDropTM. Downstream processing, quality control, and RNAseq was performed at Michael Smith laboratories facilities by 1 x Illumina seq with 150bp PET Indexed Lanes. cDNA was labelled using the Biotin Allonamide Triphosphate protocol. Target hybridization was performed at 45°C, for 16-18hr using the FS450_0001 fluidics protocol for washing. Data was acquired using the Affymetrix GeneChip Scanner 3000. CEL files were imported into R and the probe expression values were normalized using the Robust Multichip Average (RMA) method from the 'oligo' (v.1.50.0) package. Probes that were lowly expressed, defined as not having normalized expression values greater than 4 in at least 3 samples, were filtered out. Probes that ambiguously mapped to multiple genes were filtered out.

Ki-67 staining

Lentivirally transduced K562 cells were cultured in Iscove Modified Dulbecco Media with 10% FBS and antibiotics for a week after transduction. Cells were fixed and permeabilized with the BD Fixation and Permeabilization kit (#554714) according to manufacturer protocol. Fixed and permeabilized cells were stained with PE anti-human Ki-67 antibody (BioLegend #350504) diluted 1:10 in the BD Perm/Wash buffer from the kit for 30 min on ice. Unbound antibody was washed with the Perm/Wash buffer. Pelleted cells were resuspended in BD Perm/Wash buffer with 2 µg/ml DAPI and incubated for 10 min in the dark, on ice. Cells were centrifuged at 1500 x g for 5 min and resuspended in PBS with 2% FBS and strained for flow cytometry analysis.

Histology

Mouse brain samples were fixed in 10% buffered formalin and stored at 4°C for a week before paraffin embedding. H&E and myeloperoxidase staining of brain samples were performed at BC Cancer Vancouver Center Pathology office. Bone marrow smears were stained with Wright-Giemsa staining solution.

Immunoprecipitation

For co-immunoprecipitations for identifying protein-protein interactions, cells were washed in PBS then lysed with modified RIPA buffer (50 mM Tris-HCl pH 7.6, 150 mM NaCl, 1 mM EDTA, 1% Triton X-100, protease inhibitor cocktail 1 tablet/1 mL at 1:100 (Sigma-Aldrich 11697498001), phosphatase inhibitor cocktail 1:100 (Sigma-Aldrich P0044-5ML), 1 mM Na3VO4 and 10 mM NaF) for 1 hour at 4°C on a rotating platform, then passed 10x through a 22-G needle. Lysate was centrifuged at 16,000 x g for 10 min at 4°C. The supernatant was collected and protein quantification was performed using the BCA assay (BioRad DC Protein assay kit, Bio-Rad 5000112). 1 mg of protein per condition was used for co-immunoprecipitation, and the volume was made up to 1 mL with the lysis buffer. Lysate was precleared with Protein G agarose beads (EMD Millipore 16-266) for FLAG immunoprecipitation or Protein A agarose beads (EMD Millipore 16-125) for LONP1 immunoprecipitation on a rotating platform at 4°C, overnight (16 hours) for FLAG immunoprecipitation or for 3 hours for LONP1 immunoprecipitation. Beads were spun down at 1500 x g for 1 min, and the lysate was transferred to a fresh tube with 50 µL equilibrated ANTI-FLAG® M2 Affinity Gel (Sigma-Aldrich A2220-1ML) for FLAG immunoprecipitation, or with Protein A agarose beads incubated with 2 µg anti-LONP1 antibody (ThermoFisher Scientific 15440-1-AP) overnight (16 hours) and incubated on a rotating platform at 4°C for 1 hour for FLAG immunoprecipitation, and for 3 hours for LONP1 immunoprecipitation. The beads were washed with wash buffer (50 mM Tris-HCl pH 7.6, 150 mM NaCl, 0.05% Triton X-100) 5 times with 1 min 1500 x g spins in between, and eluted in 1x Laemmli sample buffer at 95°C for 15 min.
For LONP1 immunoprecipitation to identify post-translational modifications, cells are lysed with RIPA buffer (25mM Tris, 150mM NaCl, 1% NP40, 0.5% sodium deoxycholate, 0.1% sodium dodecyl sulfate (SDS) instead of modified RIPA buffer.

Quatitative tandem mass spectrometry

K562 cells lentivirally expressing FLAG-*FBXO11* were lysed in modified RIPA buffer with 10 µM MG132 (ApexBio A2585-25) as described above. Whole cell lysate was incubated with Anti-FLAG® M2 Magnetic Beads (Sigma-Aldrich M8823-1ML) or IgG beads for 3 hours then washed with lysis buffer 3 times. Three replicates per condition were directly eluted with SP3 elution buffer (200 mM HEPES pH 8.0, 10% SDS, 200 mM DTT). Four replicates each were treated with Benzonase® (EMD Millipore 70664-3) before elution. TMT labelling was performed by the mass spectrometry core at the Genome Sciences Centre. 8-plex TMT labels were used. Quantification results were calculated based on published methods[48,49].

For the set of immunoprecipitations performed without Benzonase®, proteins had normalized protein enrichment score (PESn) greater than 0.6, and were enriched in 2 of the 3 replicates by at least 1.1 fold were shortlisted. For the immunoprecipitations performed with Benzonase® treatment, proteins that had PESn greater than 0.45 and were enriched in 3 of 4 replicates by at least 1.2 fold were shortlisted. The shortlisted proteins from each experiment were intersected to identify commonly immunoprecipitated proteins.

Measuring mitochondrial membrane potential

Mitochondrial membrane potential (MMP) was measured by TMRE for cell lines (Cedarlane labs ENZ-52309), or with the JC-1 dye (eBioscience 65-0851-38) for CB.
For TMRE, cells were cultured in their regular culture media and conditions with 400 nM TMRE for 30 min. Cells were spun down at 400 x g for 5 min to remove the media and TMRE, and the cell pellets were resuspended in PBS with 2% FBS and 1 µg/mL DAPI and kept on ice before analysis by flow cytometry. JC-1 dye was used according to manufacturer protocol. Stained cells were resuspended in PBS with 2% FBS and 1 µg/mL DAPI for flow cytometry analysis.

Mitochondrial mass measurements

MitoTracker™ Deep Red FM (FisherScientific M22426) was used to measure mitochondrial mass in K562 cells. Cell staining was performed according to manufacturer protocol. Cells were stained for 30 min. Stained cells were washed with PBS with 2% FBS and resuspended in PBS with 2% FBS and 1 µg/mL DAPI for flow cytometry analysis.

Ubiquitin, neddylation activating enzyme, and proteasome inhibitor treatment

Ubiquitin activating enzyme (UAE) inhibitors PYR-41 (Sigma-Aldrich N2915-5MG) was used at 50 nM, and TAK-243 (also known as MLN7243, Selleck Chemicals S8341) at 0.1 µM. Neddylation activating enzyme (NAE) inhibitors MLN4924 (Cayman Chemical Company 15217) was used at 50 nM, and TAS4464 (Selleck Chemicals 15217) was used at 50nM. Proteasome inhibitors MG132 (ApexBio A2585) was used at 1µM, and Bortezomib (Selleck Chemicals S1013) at 50nM. Concentrations were determined by published concentrations used on K562 cells or other myeloid cell lines, and inhibitory effect on global ubiquitination or neddylation levels were confirmed by western blot. Cells were seeded at 300k cells/mL and treated with above inhibitors added directly to culture media for 16 hours. Inhibitor stock solutions were prepared in DMSO.

Western blots

Cells were washed with PBS and lysed for 30 min on a rotating platform at 4°C in RIPA buffer (25mM Tris, 150mM NaCl, 1% NP40, 0.5% sodium deoxycholate, 0.1% sodium dodecyl sulfate (SDS), protease inhibitor cocktail, phosphatase inhibitor cocktail, 1 mM Na3VO4 and 10 mM NaF). Lysed cells were centrifuged for 16,000 x g for 10 min at 4°C, and the supernatant was collected for protein quantification by BCA. Samples were mixed with Laemmli sample buffer incubated at 95°C on a heat block for 15 min.

Proteins were separated by SDS-polyacrylamide gel electrophoresis at 120 V at room temperature and transferred to nitrocellulose membrane at 100 V at room temperature for 1 hour for proteins of interest under 55 kDa, and at 35 V at 4°C for 16 hours for proteins of interest over 55 kDa. After transfer, blots were rinsed briefly with tris-buffered saline with 0.1% Tween 20 (TBST), and then blocked for 1 hour at room temperature in 5% skim milk in TBST. Membranes were washed 3 times for 10 minutes each with TBST.

Blots were probed with primary antibodies (FBXO11 antibody at 1:1000, Bethyl Laboratories A301-178A; LONP1 antibody at 1:1000, ThermoFisher Scientific 15440-1-AP; GAPDH antibody at 1:10,000, Sigma-Aldrich G8795-200UL, K63 linkage specific antibody at 1:1000, Cell Signaling Technology 5621S, NEDD8 antibody at 1:1000, Cell Signaling Technology 2745S; α-tubulin at 1:1000, Sigma-Aldrich T5168-.2ML; TOM20 at 1:1000, New England Biolabs 42406S) prepared in TBST with 1% bovine serum albumin (BSA), based on manufacturer recommended incubation times. Membranes were washed 3 times for 10 minutes each with TBST and probed with appropriate HRP secondary antibody (anti-Rabbit Immunoglobulin/HRP, Dako P044801 or aniti-mouse Immunoglobulin/HRP, Dako P0260) at 1:1000 in

TBST with 1% BSA. Blots were developed with Western Lightning Plus, Chemiluminescent Substrate (PerkinElmer NEL105) and imaged with a BioRad ChemiDoc MP Imaging system.

Seahorse XF Cell MitoStress Test

K562 wild-type control clone and *FBXO11* KO clone cells were in the growth phase at the time of the assay. The cells were counted and seeded at 80k cells per well in the 96-well Agilent Seahorse XF Cell Mito Stress Test (Agilent 103010-100) assay plate. Assay was performed as outlined in the manufacturer protocol and run on the Seahorse XFe bioanalyzer. Analysis and interpretation were done according to protocol.

BloodSpot data analysis

Transcriptomic data for SCF genes from the BloodSpot database (https://servers.binf.ku.dk/bloodspot/) were taken from GSE42519 and GSE13159 datasets. Data for *FBXO11* expression taken from the same datasets, with data for the 219208_at probe.

RNAseq analysis

RNAseq read alignment was performed using STAR aligner, and count generation was done with Salmon. Variance stabilizing transformation was performed to allow comparison between samples. Transcript per million (TPM) values were filtered to remove genes that have low counts (TPM < 0.5, equivalent to a count of 10 for the dataset) for at least 2 samples. Differential gene expression analysis was performed on the RNAseq data using DeSeq2 package with R. Gene Set Enrichment Analysis was performed using the Hallmark, C2, and C5 gene set collections from MSigDB. GSEA was performed using pre-ranked gene lists for each comparison presented, where the gene list was ranked based on the log2 fold change value. CellRadar plots from Figure 4.9 were generated using the public user interface provided by the Karlsson lab (https://karlssong.github.io/cellradar/). The same definition of differentially expressed genes was used, and HSPC data was taken from the BloodSpot HemaExplorer human normal hematopoeisis dataset.

Statistical Analysis

Measurements for experiments were taken from distinct samples. All statistical tests were performed using GraphPad Prism version 8.0 (San Diego, California). All data are presented as mean ±

standard error of the mean (SEM). Statistical significance was set at a threshold of $P < 0.05$ and FDR < 0.25.

REFERENCES

1. Döhner, H., Weisdorf, D. J. & Bloomfield, C. D. Acute Myeloid Leukemia. *N Engl J Med* **373**, 1136–1152 (2015).
2. Docking, T. R. *et al.* A clinical transcriptome approach to patient stratification and therapy selection in acute myeloid leukemia. *Nat Commun* **12**, 2474 (2021).
3. Papaemmanuil, E. *et al.* Genomic Classification and Prognosis in Acute Myeloid Leukemia. *New England Journal of Medicine* **374**, 2209–2221 (2016).
4. Walker, C. J. *et al.* Gene expression signature predicts relapse in adult patients with cytogenetically normal acute myeloid leukemia. *Blood Advances* **5**, 1474–1482 (2021).
5. Baumann, U. *et al.* Disruption of the PRKCD-FBXO25-HAX-1 axis attenuates the apoptotic response and drives lymphomagenesis. *Nat Med* **20**, 1401–1409 (2014).
6. Maser, R. S. *et al.* Chromosomally unstable mouse tumours have genomic alterations similar to diverse human cancers. *Nature* **447**, 966–971 (2007).
7. Mutations in Fbx4 Inhibit Dimerization of the SCFFbx4 Ligase and Contribute to Cyclin D1 Overexpression in Human Cancer - ScienceDirect. https://www.sciencedirect.com/science/article/pii/S1535610808001906.
8. Schieber, M. *et al.* FBXO11 is a candidate tumor suppressor in the leukemic transformation of myelodysplastic syndrome. *Blood Cancer J.* **10**, 1–12 (2020).
9. Malyukova, A. *et al.* The tumor suppressor gene hCDC4 is frequently mutated in human T-cell acute lymphoblastic leukemia with functional consequences for Notch signaling. *Cancer Res* **67**, 5611–5616 (2007).
10. Loh, M. L. *et al.* Mutations in CBL occur frequently in juvenile myelomonocytic leukemia. *Blood* **114**, 1859–1863 (2009).

11. King, B. *et al.* The ubiquitin ligase FBXW7 modulates leukemia-initiating cell activity by regulating MYC stability. *Cell* **153**, 1552–1566 (2013).
12. Reavie, L. *et al.* Regulation of hematopoietic stem cell differentiation by a single ubiquitin ligase–substrate complex. *Nat Immunol* **11**, 207–215 (2010).
13. Crusio, K. M., Reavie, L. B. & Aifantis, I. Regulation of hematopoietic stem cell fate by the ubiquitin proteasome system. *Trends Immunol* **33**, 357–363 (2012).
14. Abdel-Rahman, M. H. *et al.* Germline BAP1 mutation predisposes to uveal melanoma, lung adenocarcinoma, meningioma, and other cancers. *J Med Genet* **48**, 10.1136/jmedgenet-2011–100156 (2011).
15. Meyer, T. *et al.* Functional characterization of BRCC3 mutations in acute myeloid leukemia with t(8;21)(q22;q22.1). *Leukemia* **34**, 404–415 (2020).
16. Horton, T. M. *et al.* A Phase 2 Study of Bortezomib Combined with Either Idarubicin/Cytarabine or Cytarabine/Etoposide in Children with Relapsed, Refractory or Secondary Acute Myeloid Leukemia: A Report from the Children's Oncology Group. *Pediatr Blood Cancer* **61**, 1754–1760 (2014).
17. Tyner, J. W. *et al.* Functional genomic landscape of acute myeloid leukaemia. *Nature* **562**, 526–531 (2018).
18. Bottomly, D. *et al.* Integrative analysis of drug response and clinical outcome in acute myeloid leukemia. *Cancer Cell* (2022) doi:10.1016/j.ccell.2022.07.002.
19. Genomic and Epigenomic Landscapes of Adult De Novo Acute Myeloid Leukemia. *New England Journal of Medicine* **368**, 2059–2074 (2013).
20. Bolouri, H. *et al.* The molecular landscape of pediatric acute myeloid leukemia reveals recurrent structural alterations and age-specific mutational interactions. *Nat Med* **24**, 103–112 (2018).
21. Lindsley, R. C. *et al.* Acute myeloid leukemia ontogeny is defined by distinct somatic mutations. *Blood* **125**, 1367–1376 (2015).

22. Ma, W. *et al.* Ubiquitin-proteasome system profiling in acute leukemias and its clinical relevance. *Leuk Res* **35**, 526–533 (2011).

23. Xie, S. Z. *et al.* Sphingolipid Modulation Activates Proteostasis Programs to Govern Human Hematopoietic Stem Cell Self-Renewal. *Cell Stem Cell* **25**, 639-653.e7 (2019).

24. Xu, P. *et al.* FBXO11-mediated proteolysis of BAHD1 relieves PRC2-dependent transcriptional repression in erythropoiesis. *Blood* **137**, 155–167 (2021).

25. Higuchi, M. *et al.* Expression of a conditional AML1-ETO oncogene bypasses embryonic lethality and establishes a murine model of human t(8;21) acute myeloid leukemia. *Cancer Cell* **1**, 63–74 (2002).

26. Yuan, Y. *et al.* AML1-ETO expression is directly involved in the development of acute myeloid leukemia in the presence of additional mutations. *PNAS* **98**, 10398–10403 (2001).

27. Chou, F.-S., Wunderlich, M., Griesinger, A. & Mulloy, J. C. N-Ras(G12D) induces features of stepwise transformation in preleukemic human umbilical cord blood cultures expressing the AML1-ETO fusion gene. *Blood* **117**, 2237–2240 (2011).

28. Gibellini, L. *et al.* LonP1 Differently Modulates Mitochondrial Function and Bioenergetics of Primary Versus Metastatic Colon Cancer Cells. *Front Oncol* **8**, 254 (2018).

29. Maneix, L. *et al.* The Mitochondrial Protease LonP1 Promotes Proteasome Inhibitor Resistance in Multiple Myeloma. *Cancers (Basel)* **13**, 843 (2021).

30. Quirós, P. M. *et al.* ATP-Dependent Lon Protease Controls Tumor Bioenergetics by Reprogramming Mitochondrial Activity. *Cell Reports* **8**, 542–556 (2014).

31. Ghosh, J. C. *et al.* Akt phosphorylation of mitochondrial Lonp1 protease enables oxidative metabolism and advanced tumor traits. *Oncogene* **38**, 6926–6939 (2019).

32. Mansell, E. *et al.* Mitochondrial Potentiation Ameliorates Age-Related Heterogeneity in Hematopoietic Stem Cell Function. *Cell Stem Cell* **28**, 241-256.e6 (2021).

33. Romero-Moya, D. *et al.* Cord blood-derived CD34+ hematopoietic cells with low mitochondrial mass are enriched in hematopoietic repopulating stem cell function. *Haematologica* **98**, 1022–1029 (2013).

34. Vannini, N. *et al.* Specification of haematopoietic stem cell fate via modulation of mitochondrial activity. *Nat Commun* **7**, 13125 (2016).

35. Abida, W. M., Nikolaev, A., Zhao, W., Zhang, W. & Gu, W. FBXO11 Promotes the Neddylation of p53 and Inhibits Its Transcriptional Activity. *J Biol Chem* **282**, 1797–1804 (2007).

36. Liu, M. *et al.* Macrophage K63-Linked Ubiquitination of YAP Promotes Its Nuclear Localization and Exacerbates Atherosclerosis. *Cell Reports* **32**, (2020).

37. Duan, S. *et al.* FBXO11 targets BCL6 for degradation and is inactivated in diffuse large B-cell lymphomas. *Nature* **481**, 90–93 (2012).

38. Rossi, M. *et al.* Regulation of the CRL4(Cdt2) ubiquitin ligase and cell-cycle exit by the SCF(Fbxo11) ubiquitin ligase. *Mol Cell* **49**, 1159–1166 (2013).

39. Jin, Y. *et al.* FBXO11 promotes ubiquitination of the Snail family of transcription factors in cancer progression and epidermal development. *Cancer Letters* **362**, 70–82 (2015).

40. Cole, A. *et al.* Inhibition of the Mitochondrial Protease ClpP as a Therapeutic Strategy for Human Acute Myeloid Leukemia. *Cancer Cell* **27**, 864–876 (2015).

41. Gibellini, L. *et al.* Chapter One - The biology of Lonp1: More than a mitochondrial protease. in *International Review of Cell and Molecular Biology* (ed. Galluzzi, L.) vol. 354 1–61 (Academic Press, 2020).

42. Shin, C.-S. *et al.* LONP1 and mtHSP70 cooperate to promote mitochondrial protein folding. *Nat Commun* **12**, 265 (2021).

43. Choi, C. H., Zimon, A. & Usheva, A. Metabolic stress regulates basic transcription through acetyl-coenzyme A. *CMLS, Cell. Mol. Life Sci.* **62**, 625 (2005).

44. Martín-Martín, N., Carracedo, A. & Torrano, V. Metabolism and Transcription in Cancer: Merging Two Classic Tales. *Frontiers in Cell and Developmental Biology* **5**, 119 (2018).

45. Sanin, D. E. *et al.* Mitochondrial Membrane Potential Regulates Nuclear Gene Expression in Macrophages Exposed to Prostaglandin E2. *Immunity* **49**, 1021-1033.e6 (2018).

46. Cheng, D. T. *et al.* Memorial Sloan Kettering-Integrated Mutation Profiling of Actionable Cancer Targets (MSK-IMPACT). *J Mol Diagn* **17**, 251–264 (2015).

47. Jaiswal, S. *et al.* Age-Related Clonal Hematopoiesis Associated with Adverse Outcomes. *New England Journal of Medicine* **371**, 2488–2498 (2014).

48. Griffin, N. M. *et al.* Label-free, normalized quantification of complex mass spectrometry data for proteomic analysis. *Nat Biotechnol* **28**, 83–89 (2010).

49. Lavallée-Adam, M., Rauniyar, N., McClatchy, D. B. & Yates, J. R. PSEA-Quant: A Protein Set Enrichment Analysis on Label-Free and Label-Based Protein Quantification Data. *J. Proteome Res.* **13**, 5496–5509 (2014).

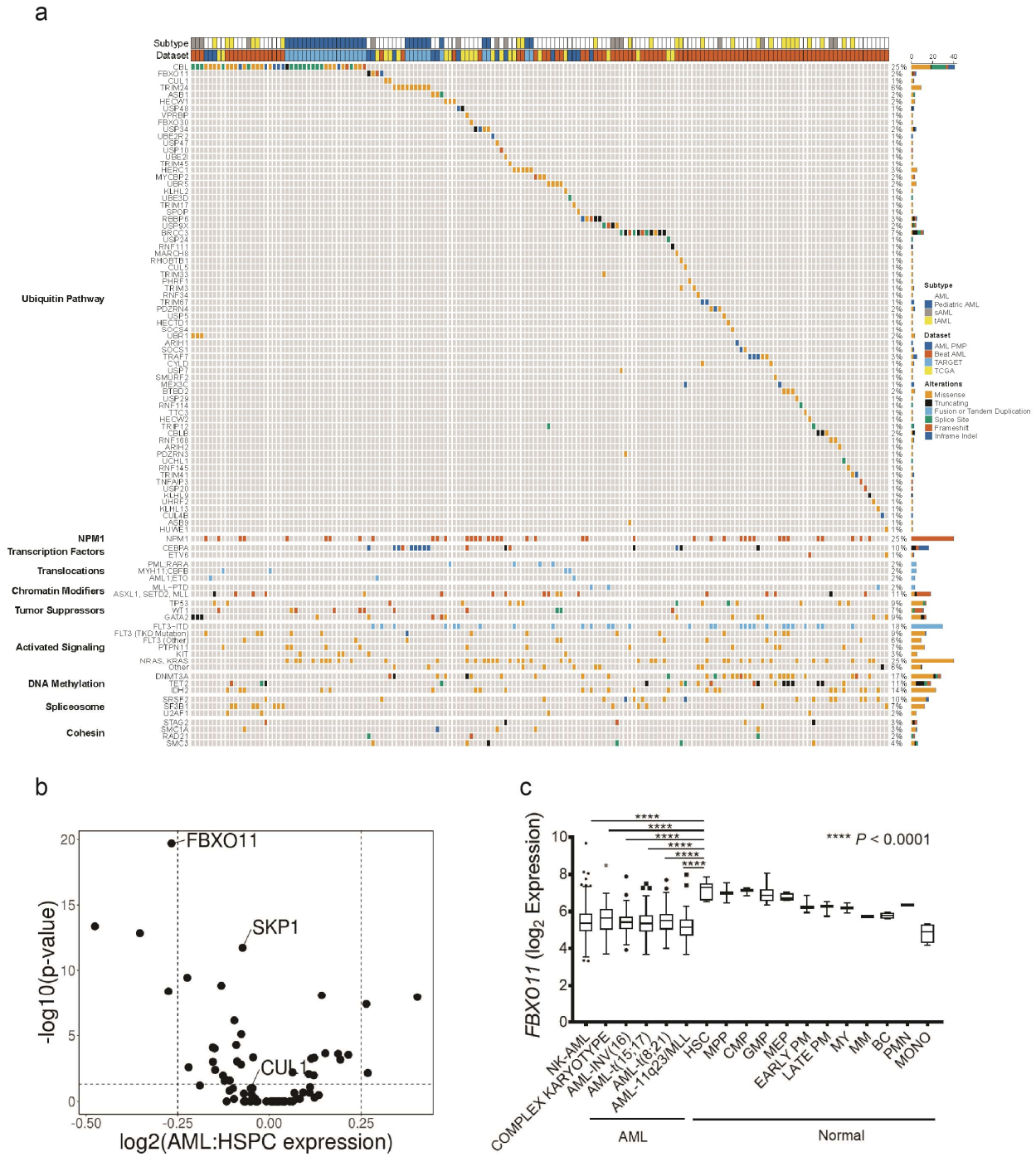

Figure 1. Aberration of ubiquitin pathway gene sequence or expression is frequent in AML

a, AML patients with ubiquitin pathway mutations from AML PMP, TCGA, TARGET, and Beat AML data sets are represented in an oncoprint. Shown are 163 of 1,627 AML patients with ubiquitin pathway mutations along with co-occurring somatic mutations. Columns represent individual AML samples, and rows represent individual genes. **b**, Shown is a volcano plot comparing transcript expression of SCF genes. Bonferroni-adjusted *P* values represent *t*-tests. The horizontal dotted line represents *P* = 0.05. Vertical lines represent $\log_2$ fold change of |0.25|. **c**, Expression levels of *FBXO11* transcripts across

different AML subtypes and normal hematopoietic populations from BloodSpot are represented as a box and whisker plot. The median is shown with a horizontal line, with the edges of the box corresponding to the first and third quartiles of the distribution, with whiskers extending to 1.5* the inter-quartile range of the distribution. *P* values represent two-tailed *t*-tests.

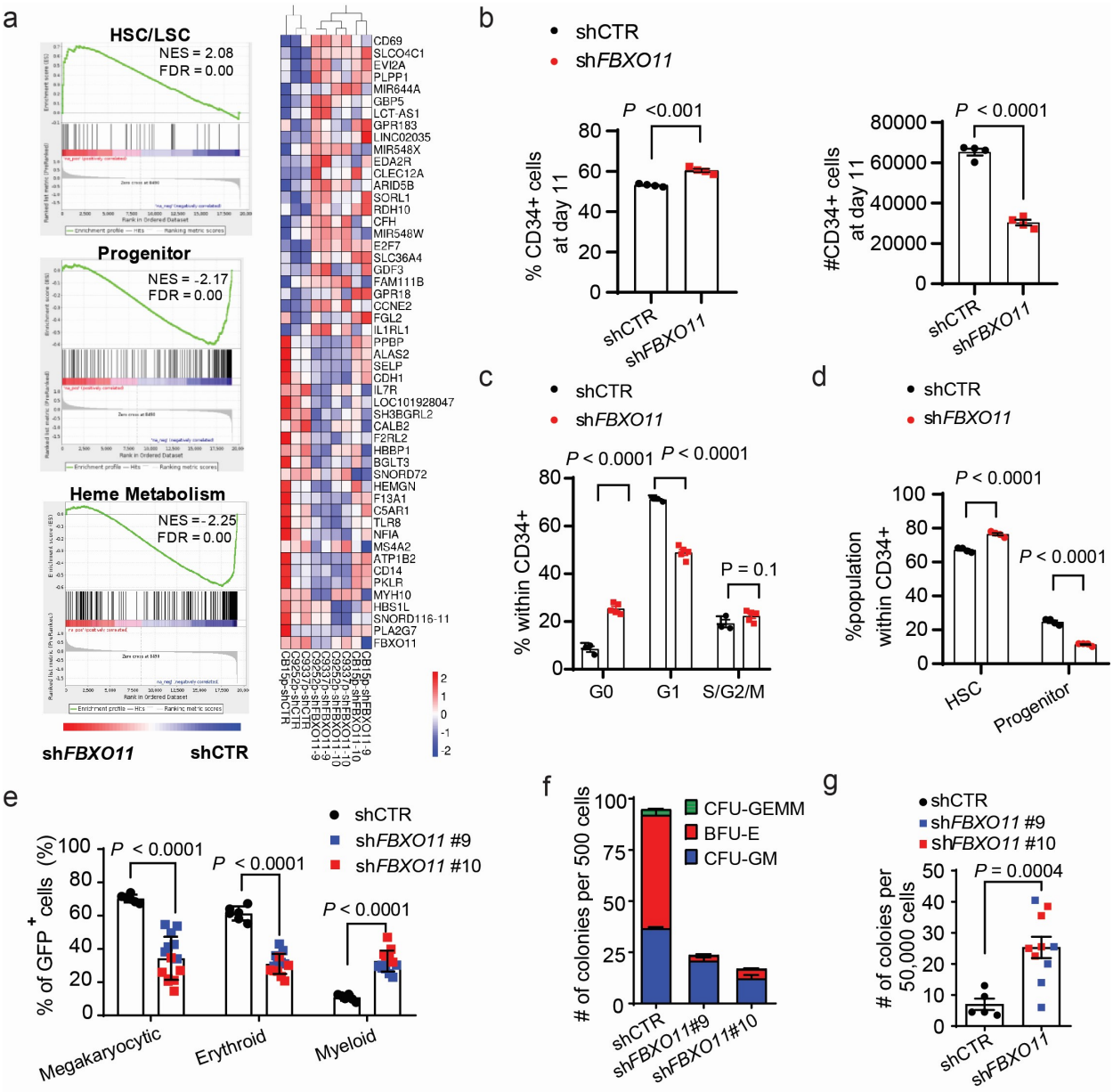

Figure 2. *FBXO11* depletion promotes quiescence and blocks differentiation.

a, Shown are Gene Set Enrichment Analysis plots for the EPPERT_CE_HSC_LSC (HSC/LSC), EPPERT_PROGENITOR (Progenitor), and HALLMARK_HEME_METABOLISM (Heme Metabolism) gene sets comparing CD34$^+$ HSPC with *FBXO11* depletion (sh*FBXO11*) to cells expressing non-targeting control shRNA (shCTR). The heatmap on the right is arranged according to pairwise clustering based on the 25 most upregulated and 25 most downregulated genes in *FBXO11*-depleted cells compared to control. **b**,

Shown are percentages and absolute cell counts of CD34$^+$ HSPC expressing shCTR or sh*FBXO11* at day 7 of culture (*n* = 4 independent replicates). **c**, Cell cycle state of CD34$^+$ HSPC was measured by Ki-67/DAPI staining (*n* = 3 (shCTR), *n* = 5 (sh*FBXO11*) independent replicates). **d**, Percentages of CD45RA$^-$ (corresponding to cultured HSC immunophenotype) and CD45RA$^+$90$^-$ (corresponding to cultured hematopoietic progenitor (HPC) immunophenotype) cells within the CD34$^+$ population are shown (*n* = 4 (shCTR), *n* = 4 (sh*FBXO11*) independent replicates). **e**, Shown are percentages of megakaryocytic (CD41$^+$ CD61$^+$), erythroid (CD71$^+$ Glycophorin A/B$^+$), and myeloid (CD15$^+$) cells in CD34$^+$ HSPC expressing shCTR or sh*FBXO11* after 7 days of culture. **f**, Primary CFC from CD34$^+$ HSPC expressing shCTR or sh*FBXO11* were counted 12 days after plating (*n* = 5 independent replicates). **g**, Colony counts following secondary plating of 50,000 cells from the primary CFC assay shown in panel (f) (*n* = 5 independent replicates). *P* values represent two-tailed *t*-test, and error bars represent s.d.

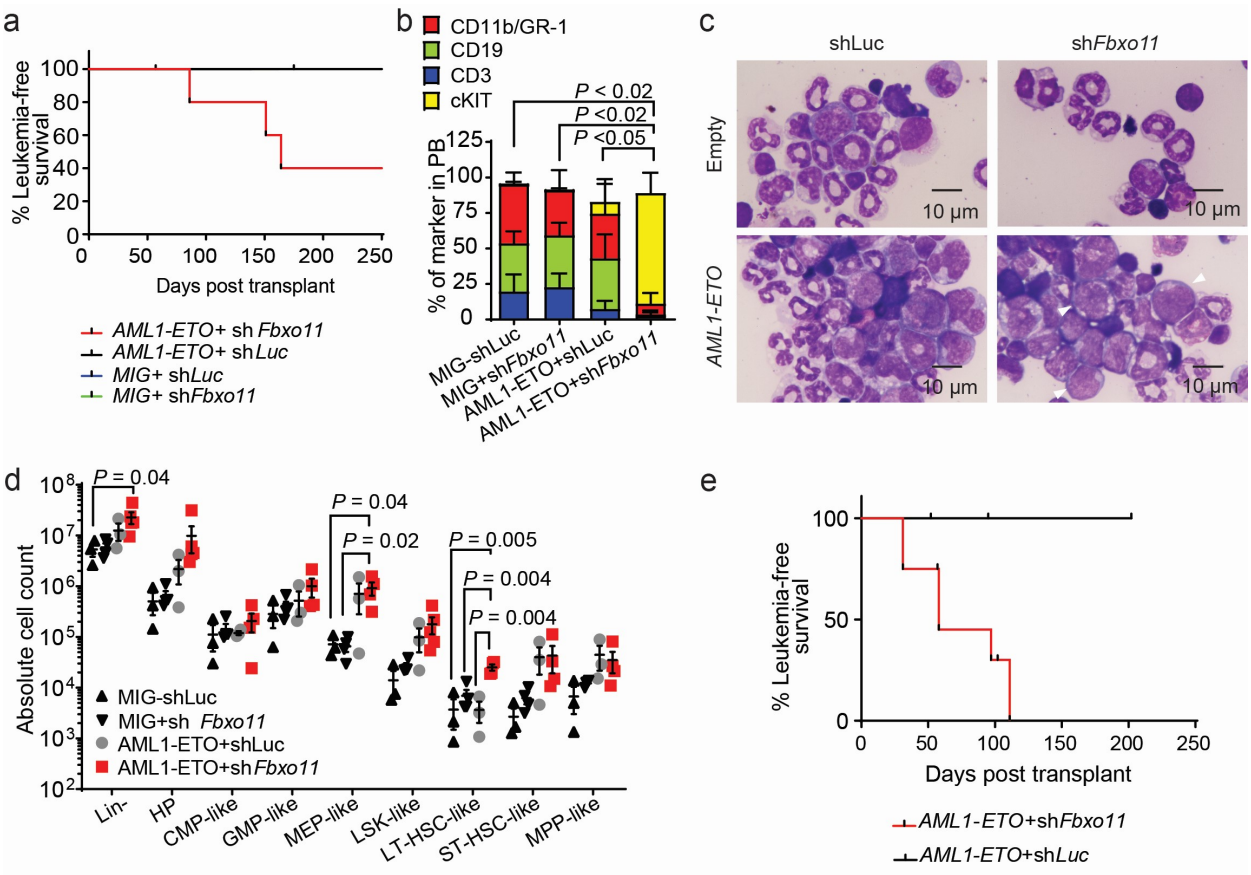

Figure 3. *Fbxo11* depletion cooperates with *AML1-ETO* to generate AML in mice.
a, The Kaplan-Meier plot shows survival data for mice transplanted with HSPC expressing *AML1-ETO* fusion cDNA or empty vector (MIG) and retrovirus expressing an shRNA against murine *Fbxo11* (sh*Fbxo11*) or control shRNA against luciferase (shLuc) (*n* = 4-5 mice). *P* = 0.06 for *AML1-ETO* + sh*Fbxo11*vs *AML1-ETO* + sh*Luc* (Mantel-Cox test). **b**, Peripheral blood cell expression of myeloid (CD11/GR-1), B-cell (CD19), T-cell (CD3), and myeloid progenitor (lineage-negative, c-KIT positive) surface markers were measured at endpoint by flow cytometry. **c**, Giemsa-stained bone marrow

cytospins from representative animals from panel (a) at endpoint. Arrows point to blast cells. **d**, Absolute cell counts of bone marrow cells expressing cell surface markers corresponding to normal HSPC populations were determined by flow cytometry. Flow cytometry data and gating strategies are shown in Supplementary Figure 6. *P* values represent two-tailed *t*-tests, and error bars represent s.d. **e**, Shown are Kaplan-Meier curves following secondary bone marrow transplantation of marrow from 2-4 different primary transplanted animals from panel (a) (*n* = 4-8 mice); *P* = 0.07 (Mantel-Cox test)).

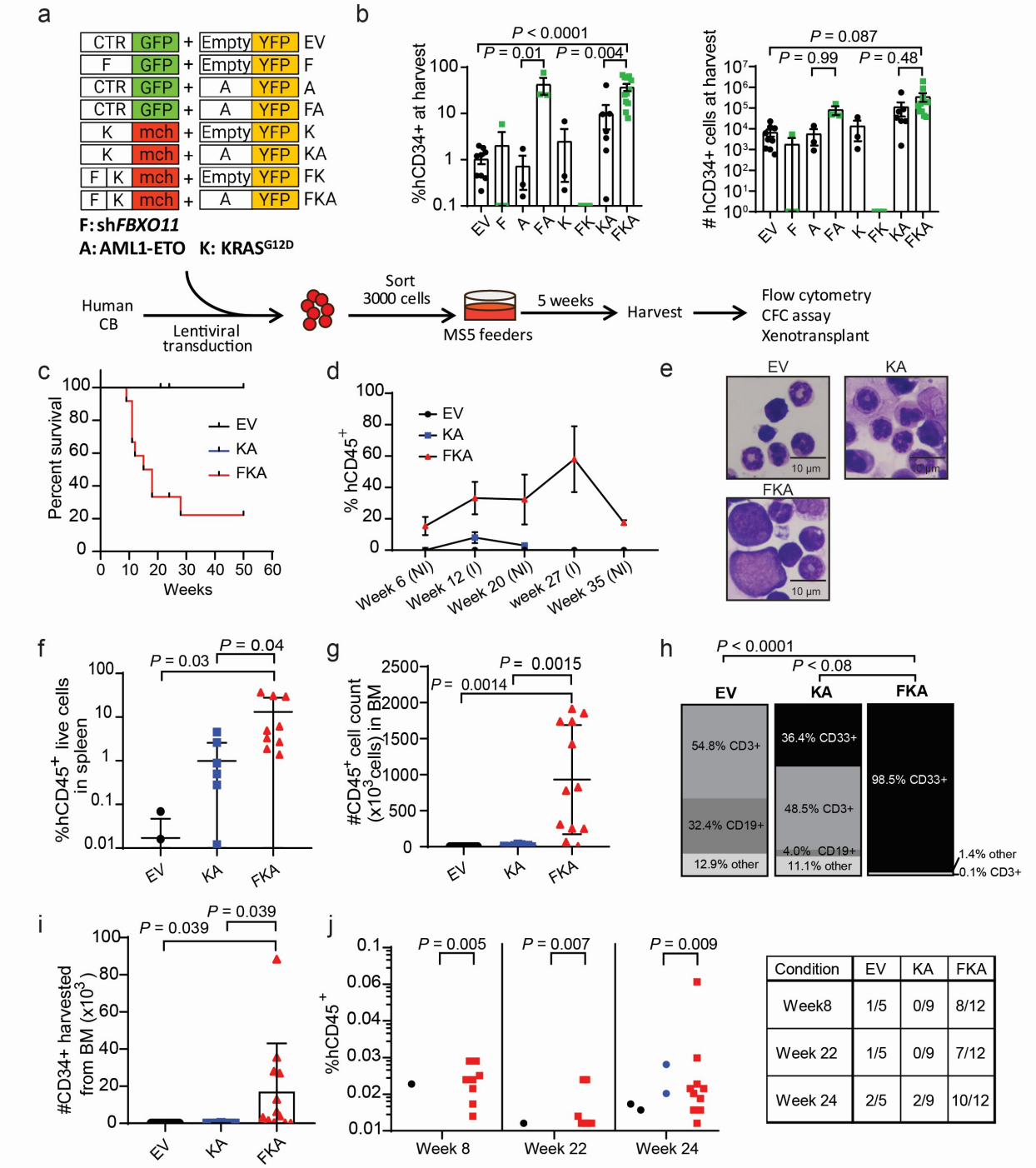

Condition	EV	KA	FKA
Week8	1/5	0/9	8/12
Week 22	1/5	0/9	7/12
Week 24	2/5	2/9	10/12

Figure 4. *FBXO11* depletion cooperates with *AML1-ETO* and *KRAS*^{G12D} to generate human myeloid leukemia.

a, Schematic outlining the experimental design for long-term culture and xenotransplant of CD34$^+$ HSPC. **b**, *FBXO11* knockdown maintains CD34$^+$ cells in long-term culture. Percentages (left panel) and total live cell counts (right panel) of CD34$^+$ cells were measured on day 40 of culture (*n* = 9 (EV), *n* = 3 (F, A, FA, K, FK), n = 7 (KA), *n* = 12 (FKA) independent replicates). **c**, Kaplan-Meier curve for mice transplanted with cells harvested in (b) (*P* = 0.0028 for EV vs FKA, and *P* = 0.0002 for KA vs FKA (Mantel-Cox test)). **d**, Bone marrow engraftment of transduced CD34$^+$ cells harvested in (b) (EV, empty vector + control shRNA (*n* = 13); KA, *KRAS*^{G12D} + *AML1-ETO* (*n* = 9); and FKA, sh*FBXO11* + *KRAS*^{G12D} + *AML1-ETO* (*n* = 12) mice) showing CD45$^+$ cell chimerism levels in the non-injected bone (NI) or injected bone (I) (*P* = 0.0033 for EV vs FKA, *P* = 0.018 for KA vs FKA (Sidak's multiple comparisons test)). **e**, Giemsa-stained bone marrow smear from mice at endpoint. **f**, Human CD45$^+$ hematopoietic cell engraftment in the spleen at endpoint as percentage of total viable spleen cells (*n* = 5 (EV, 3 not detected (ND)), *n* = 9 (KA, 1 ND), *n* = 9 (FKA) mice). **g**, Human CD45$^+$ hematopoietic cell engraftment in the bone marrow measured at endpoint. (*n* = 13 (EV, 7 ND), *n* = 9 (KA), *n* = 12 (FKA) mice). **h**, Percentage of lymphoid (CD3$^+$, CD19$^+$), myeloid (CD33$^+$), and other (CD3$^-$ CD19$^-$ CD33$^-$) cells within the viable human CD45$^+$ cell population was measured in bone marrow cells at endpoint. (*n* = 5 (EV), *n* = 5 (KA), *n* = 5 (FKA) mice). **i**, Total CD34$^+$ HSPC numbers in the bone marrow were quantified at endpoint. (*n* = 13 (EV, 13 ND), *n* = 9 (KA, 8 ND), *n* = 12 (FKA) mice). **j**, Hematopoietic cell engraftment in secondary transplants was assessed at weeks 8, 22 and 24. The table on the right lists the fraction of mice in each condition with detectable engraftment at each time point (*P* values represent Fisher's exact tests). All *P* values represent two-tailed *t*-tests unless otherwise specified, and error bars represent s.d.

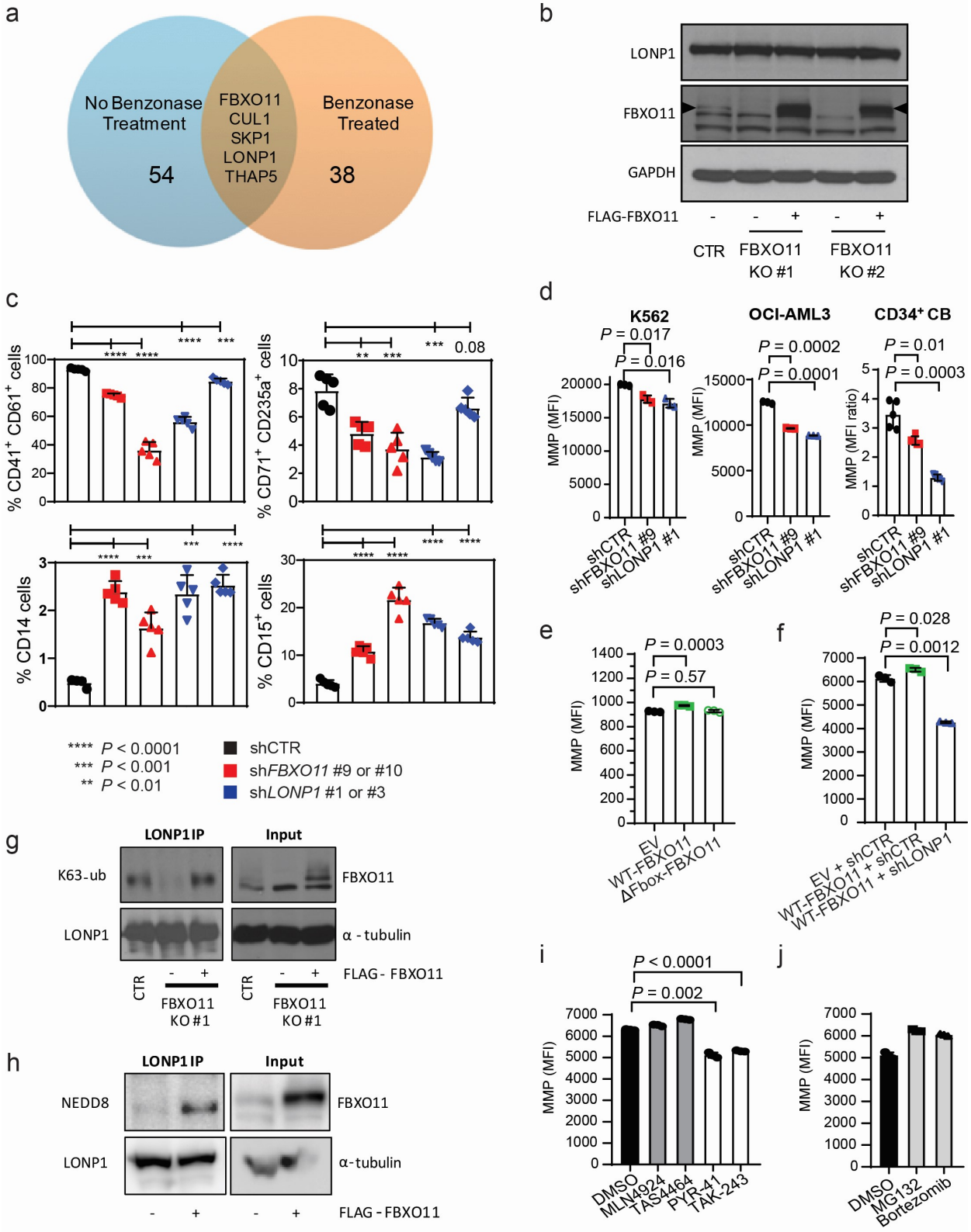

Figure 5. FBXO11 regulates mitochondrial function through activation of LONP1.

a, Proteins coimmunoprecipitated with FLAG-FBXO11 in K562 cells with or without Benzonase® treatment (*n* = 3 to 4 independent replicates). **b**, Whole cell lysates from K562 parental cells (CTR) or *FBXO11* KO CRISPR clones expressing empty vector or FLAG-tagged FBXO11 (FLAG-FBXO11) were immunoblotted as indicated. **c**, Viable $CD34^+$ HSPC expressing control shRNA (shCTR), sh*FBXO11* or sh*LONP1* were assessed for megakaryocyte ($CD41^+CD61^+$), erythroid ($CD71^+CD235a^+$) or myeloid ($CD14^+$ or $CD15^+$) cell surface markers after 7 days of culture (*n* = 4-5 independent replicates). **d**, MMP measured in K562 and OCI-AML3 cells and $CD34^+$ HSPC expressing shRNA targeting *FBXO11* or *LONP1* (*n* = 3 independent replicates). **e**, MMP measured in K562 cells expressing WT *FBXO11* or *FBXO11* with deleted F-box domain (ΔFbox-FBXO11) (*n* = 3 independent replicates). **f**, MMP measured in K562 cells expressing EV with control shRNA (shCTR), or WT-FBXO11 co-expressed with shCTR or shRNA targeting *LONP1* (shLONP1). **g**, Immunoblots of K63-linked polyubiquitination or **h**, neddylation (NEDD8) of LONP1 immunoprecipitated from parental K562 cells (CTR) or an *FBXO11* CRISPR KO clone expressing empty vector or FLAG-FBXO11. **i**, MMP measured in K562 cells expressing WT-FBXO11 treated with vehicle (DMSO), neddylation activating enzyme inhibitors (MLN4924 or TAS4464), ubiquitin activating enzyme inhibitors (PYR-41 or TAK-243), or **j,** proteasome inhibitors (MG132 or Bortezomib) (*n* = 3 independent replicates). *P* values represent two-tailed *t*-tests. Error bars represent s.d.

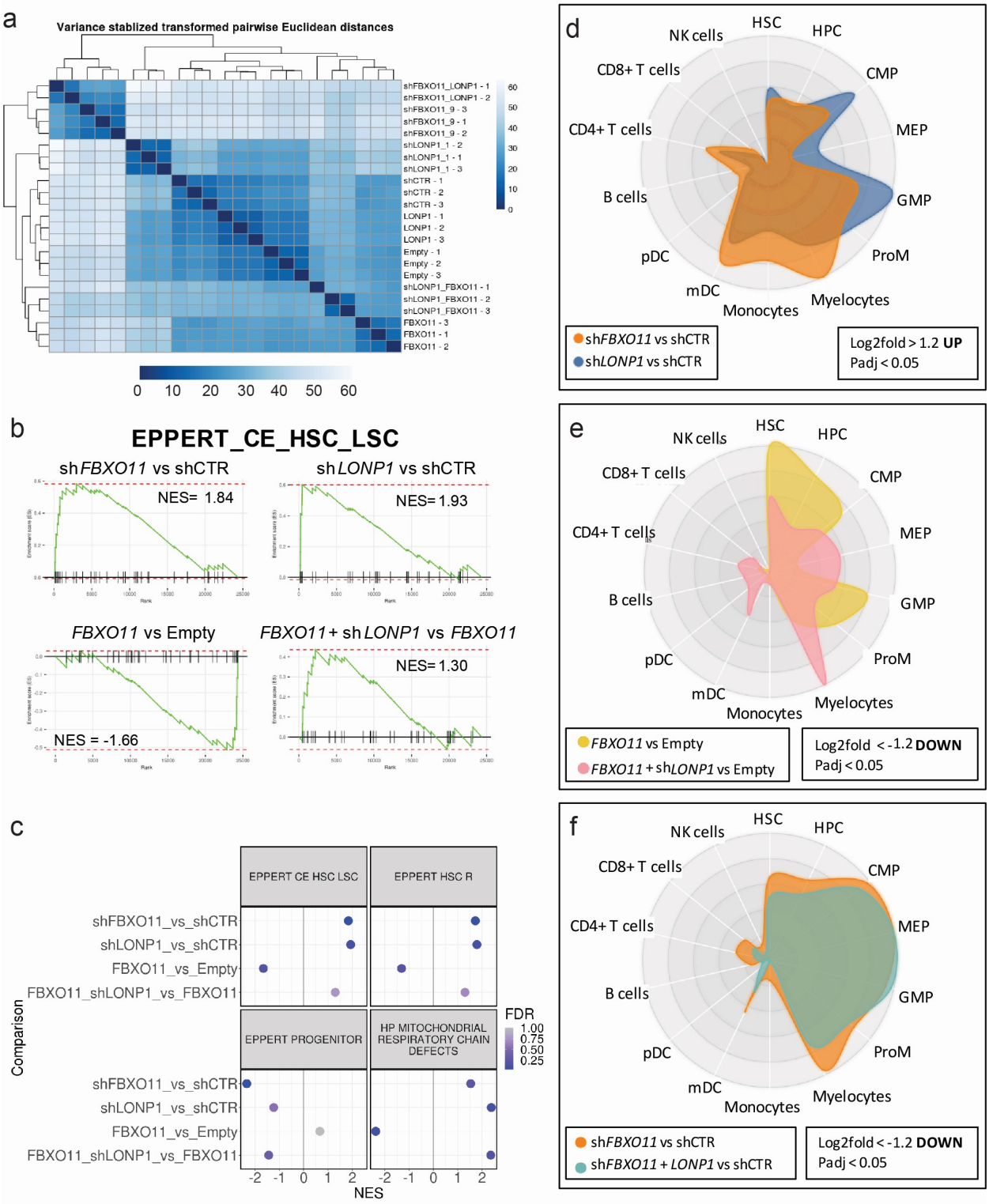

Figure 6. *LONP1* is required for functional effects of *FBXO11*.

RNA-seq data from CD34$^+$ HSPC expressing shCTR, sh*FBXO11*, sh*LONP1*, empty vector (Empty or EV), FBXO11, LONP1, FBXO11 with sh*LONP1*, or LONP1 with sh*FBXO11* (*n* = 3 independent replicates except

for LONP1 + sh*FBXO11* (*n* = 2 independent replicates)). **a**, Heatmap represents pair-wise Euclidian distances between samples based on expression of all detected genes. **b**, GSEA enrichment plots for the EPPERT_CE_HSC_LSC gene set is shown for various comparisons as noted. **c**, Enrichment trends of various GSEA genesets are summarized for the comparisons listed. Normalized enrichment scores (NES) for each condition are plotted. The false discovery rate (FDR) is represented by the color scale. **d-f**, Cell radar plots were generated using human normal hematopoiesis (HemaExplorer) data from the Bloodspot database. The enrichment of genes associated with different hematopoietic populations indicated are compared between different groups as listed. The closer the outline is to the edge of the plot at a labelled point, the greater the proportion of differentially expressed genes associated with the corresponding cell population. Thresholds for differential gene expression were set at $\log_2$fold > |1.2| and adjusted $P < 0.05$. **d**, Shown are proportions of genes associated with various hematopoietic populations upregulated with *FBXO11* or *LONP1* knockdown compared to control shRNA. **e**, Shown are proportions of genes associated with various hematopoietic populations downregulated with WT *FBXO11* expression, or with *FBXO11* expression combined with *LONP1* knockdown, relative to empty vector control. **f**, Shown are proportions of genes associated with various hematopoietic populations down regulated with *FBXO11* knockdown, or with *FBXO11* knockdown combined with *LONP1* expression, relative to control shRNA.

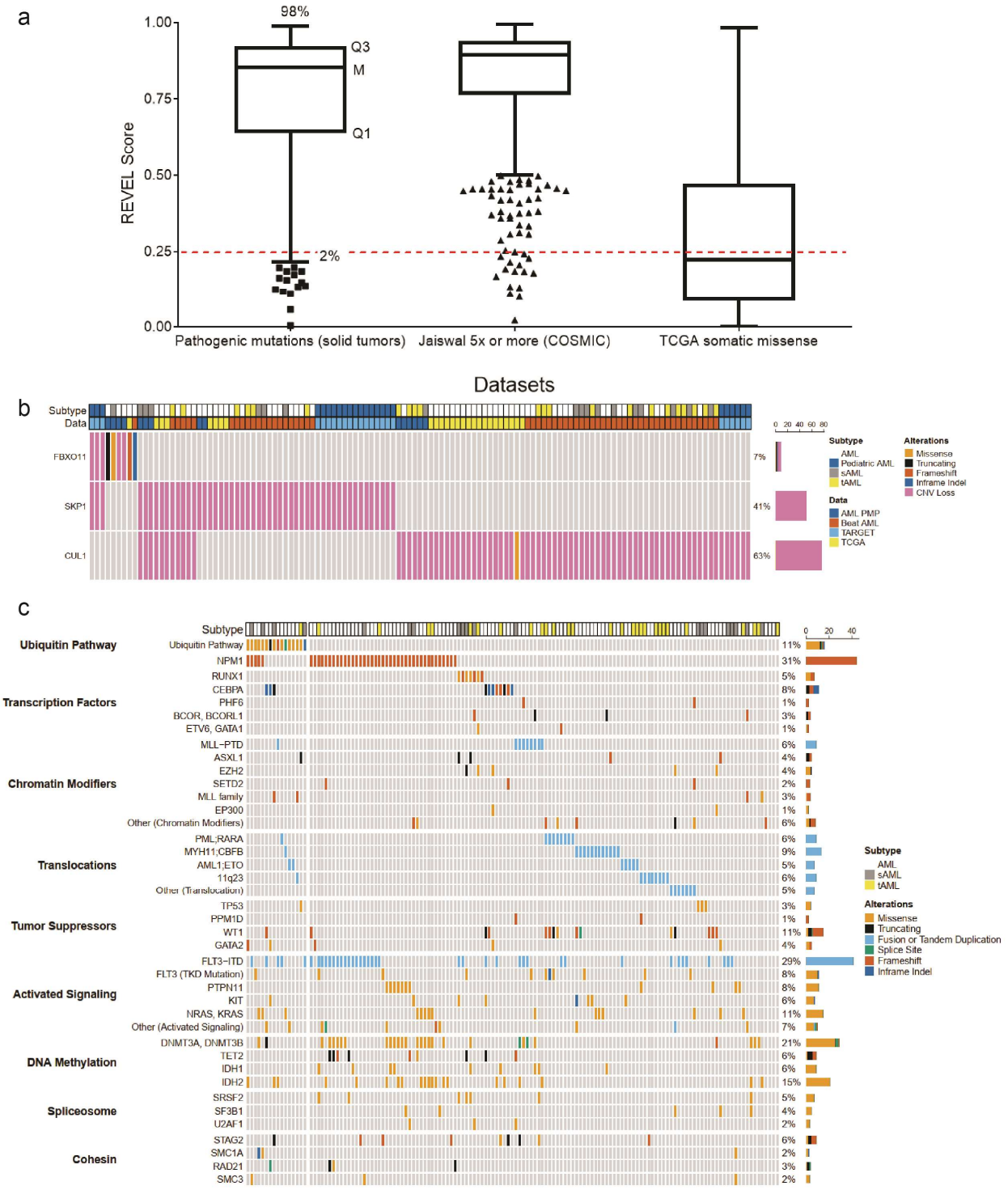

Supplementary Figure 1. Mutations affecting the ubiquitin pathway occur frequently in AML.
a, REVEL scores for different mutation datasets were compared to identify a threshold for pathogenicity prediction. Mutations plotted include: (1) Known actionable pathogenic missense variants in solid tumors (*n* = 146 variants). (2) Pathogenic variants associated with human hematological cancers

(Jaiswal)[47] (*n* = 149 variants). (3) Somatic missense mutations in AML identified in TCGA[19] (*n* = 1233 mutations). Applying a minimal REVEL threshold of 0.250, represented by the red dotted horizontal line, removes more than half of all identified somatic missense TCGA variants, while retaining 98% of known pathogenic variants. **b**, Variants affecting the SCF^{FBXO11} complex are summarized in the oncoprint. In the combined AML PMP, TCGA, Beat AML and TARGET pediatric AML datasets, 123 of 1,627 AML patients (8%) had a mutation or copy loss of a gene affecting the SCF^{FBXO11} complex. **c**, Somatic mutations that satisfy REVEL scores > 0.250 and CADD scores > 10.5 in AML PMP and TCGA AML samples are summarized in the oncoprint. Patients with one or more mutations affecting genes belonging to the ubiquitin pathway are grouped together to the left. AML: *de novo* AML, sAML: transformed AML derived from myelodysplastic syndrome (MDS), tAML: therapy-related AML.

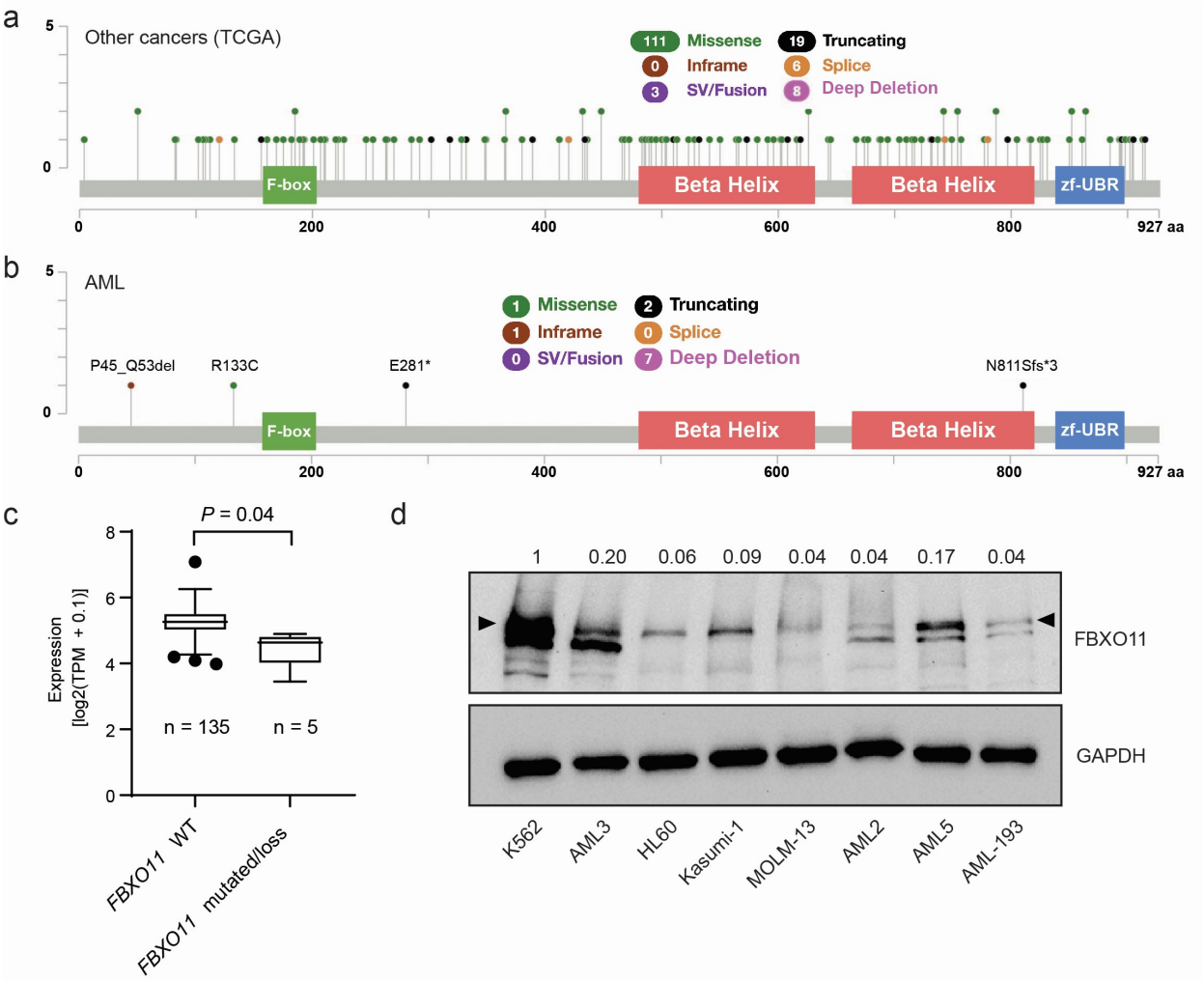

Supplementary Figure 2. *FBXO11* is recurrently mutated in multiple cancers.
a, *FBXO11* mutation types, locations, and frequencies identified in all TCGA cancer samples (n = 10,753) excluding AML samples are shown (cBioPortal). **b**, *FBXO11* mutation types, locations, and frequencies identified in TCGA, Beat AML, TARGET pediatric AML, and AML PMP samples. **c**, *FBXO11* transcript expression in AML PMP samples with mutated/deleted (*FBXO11* mutated/loss) *FBXO11* or WT *FBXO11*

represented as a box and whisker plot. **d**, Various myeloid cell lines were immunoblotted for FBXO11 expression. *P* values represent two-tailed *t*-tests and error bars represent s.d.

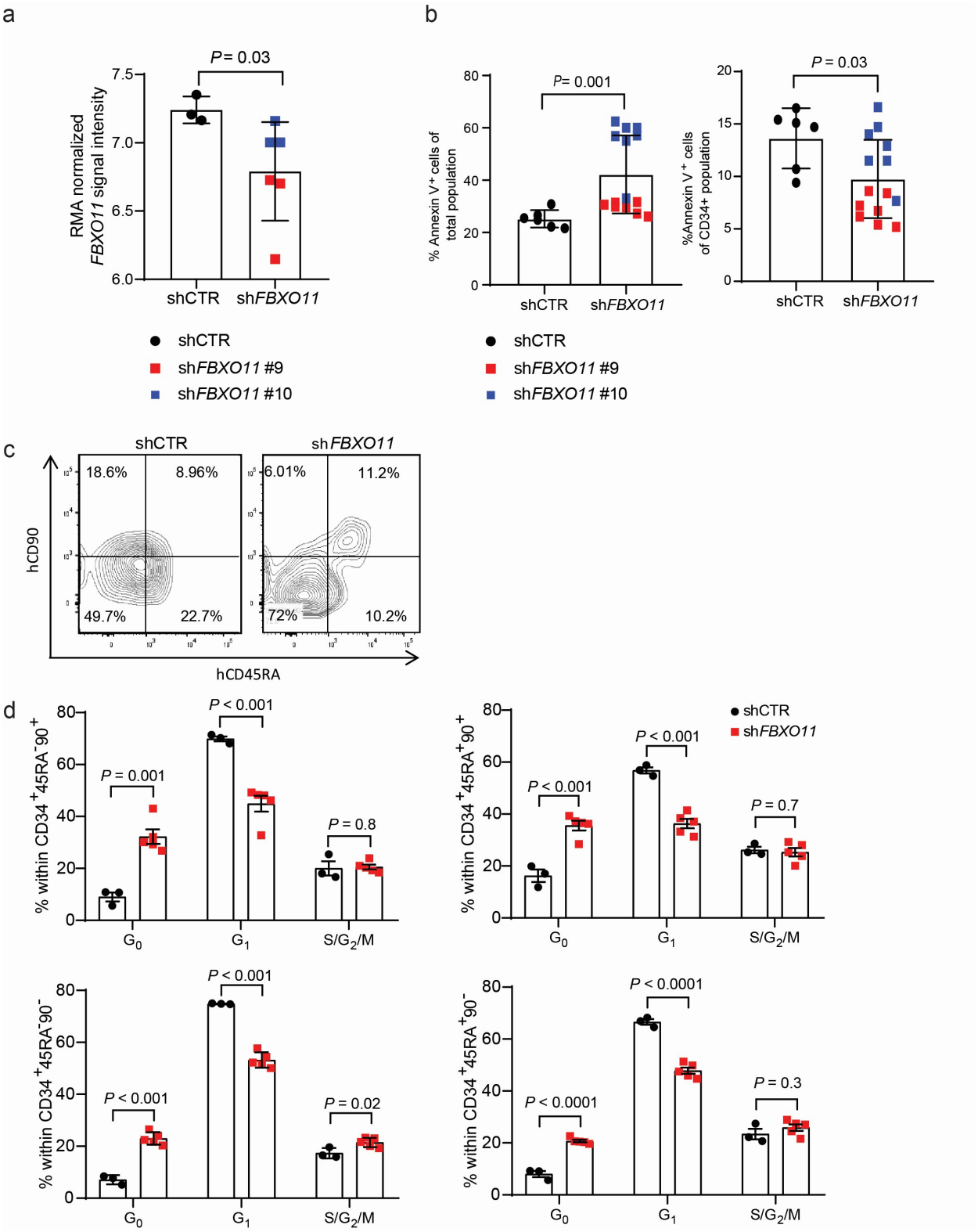

Supplementary Figure 3. CD34$^+$ HSPC with *FBXO11* depletion have reduced cell death.
a, Robust multiarray averaging (RMA) normalized *FBXO11* signal intensity in CD34$^+$ HSPC samples (n = 3 independent replicates). **b**, The Annexin V$^+$ population within total (left) or CD34$^+$ (right) cells was analyzed by flow cytometry (n = 6 (shCTR), n = 7 (sh*FBXO11*) independent replicates). **c**, Representative plot of cultured CD34$^+$ HSPC analyzed for expression of long-term and short-term HSC (CD90$^{+/-}$CD45RA$^-$) or progenitor (CD90$^-$CD45RA$^-$) markers. P values represent two-tailed t-tests and error bars represent s.d. **d**, Cell cycle states of the HSPC populations were determined by Ki-67 staining (n = 3 (shCTR), n = 5 (sh*FBXO11*) independent replicates).

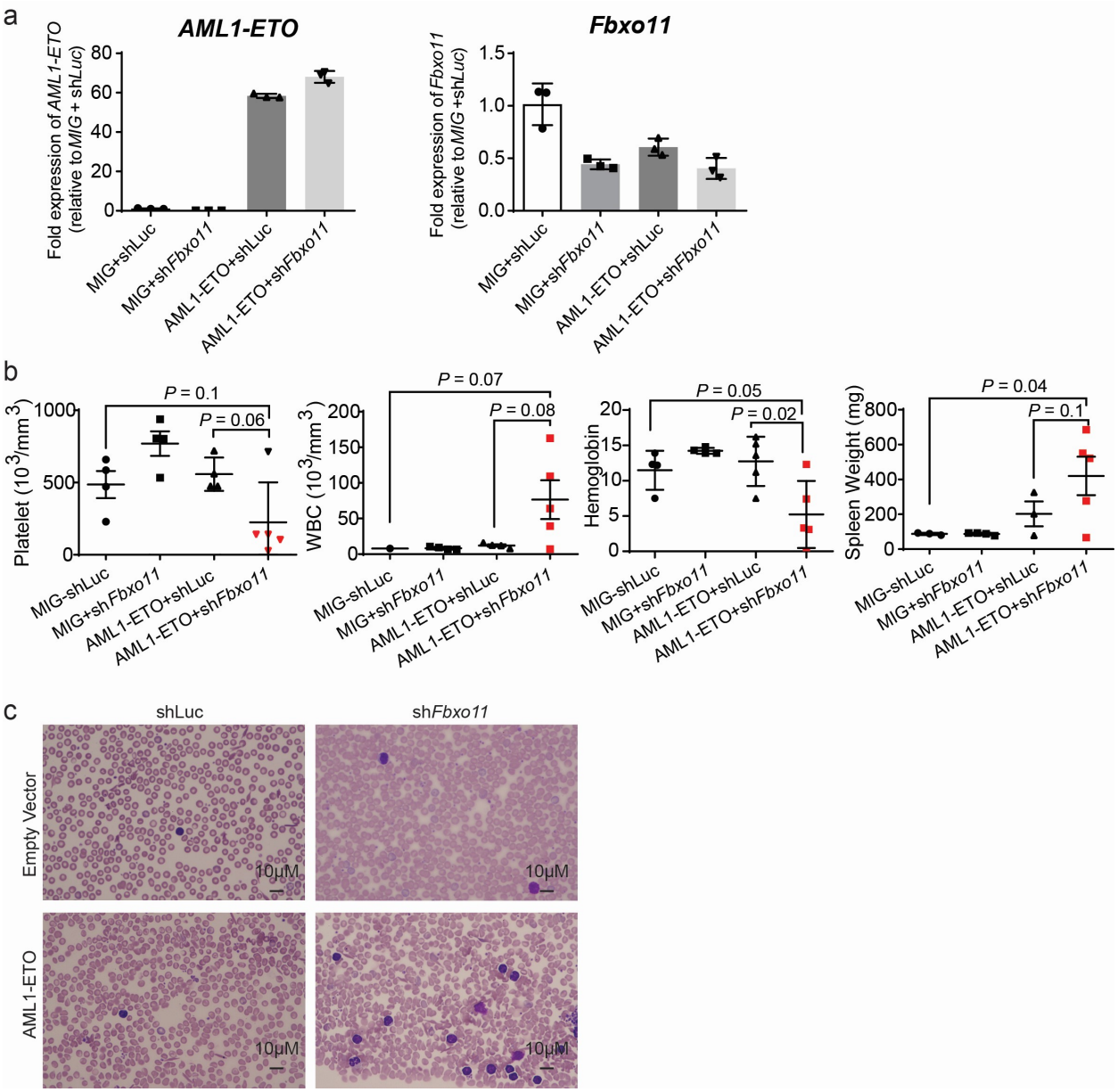

Supplementary Figure 4. *Fbxo11* depletion cooperates with *AML1-ETO* expression to promote leukemogenesis.

a, *AML1-ETO* overexpression and *Fbxo11* knockdown in transduced bone marrow cells were confirmed by RT-qPCR. **b**, Peripheral blood counts and spleen weights were measured at endpoint (n = 3-5, except for n = 1 for MIG-shLuc WBC. P values represent two-tailed t-tests and error bars represent s.d.). **c**, Giemsa stains were performed on peripheral blood smears prepared at endpoint.

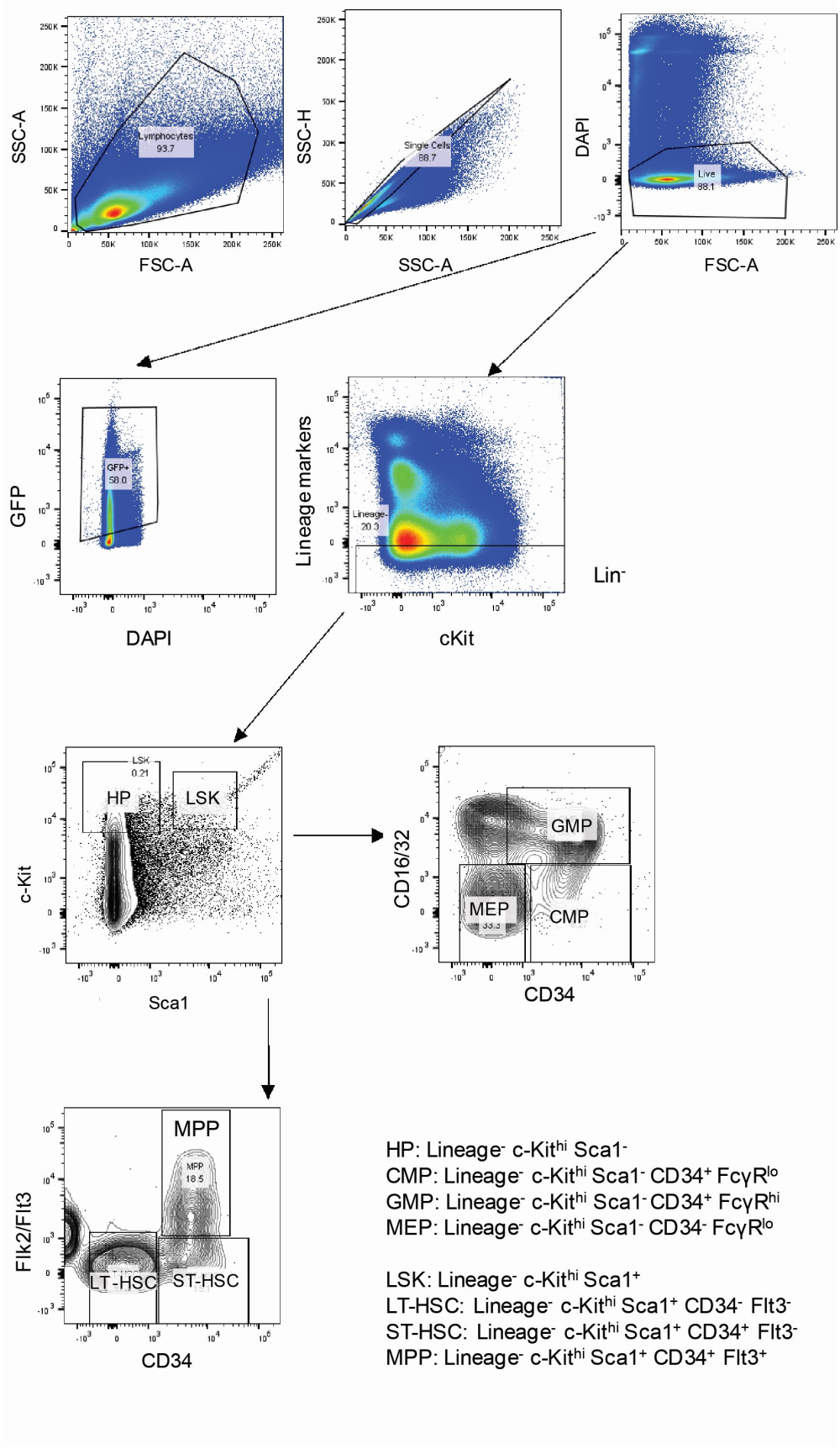

HP: Lineage$^-$ c-Kit^{hi} Sca1$^-$
CMP: Lineage$^-$ c-Kit^{hi} Sca1$^-$ CD34$^+$ FcγR^{lo}
GMP: Lineage$^-$ c-Kit^{hi} Sca1$^-$ CD34$^+$ FcγR^{hi}
MEP: Lineage$^-$ c-Kit^{hi} Sca1$^-$ CD34$^-$ FcγR^{lo}

LSK: Lineage$^-$ c-Kit^{hi} Sca1$^+$
LT-HSC: Lineage$^-$ c-Kit^{hi} Sca1$^+$ CD34$^-$ Flt3$^-$
ST-HSC: Lineage$^-$ c-Kit^{hi} Sca1$^+$ CD34$^+$ Flt3$^-$
MPP: Lineage$^-$ c-Kit^{hi} Sca1$^+$ CD34$^+$ Flt3$^+$

Supplementary Figure 5. Gating strategy for bone marrow flow cytometry analysis at end point.

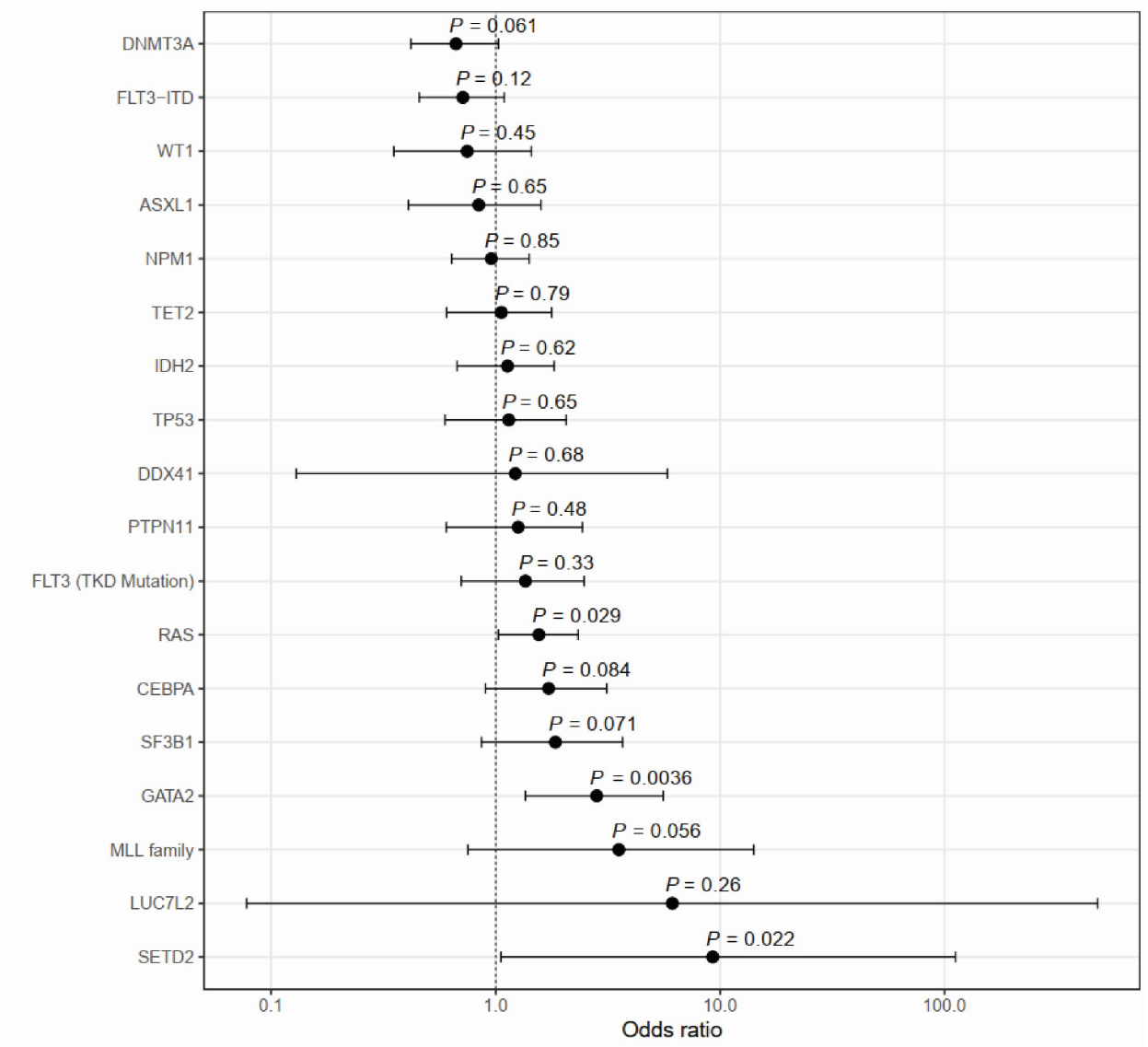

Supplementary Figure 6. Ubiquitin pathway mutations cooccur with *RAS, GATA2,* and *SETD2* mutations.

Shown are odds ratios of AML-associated mutations for AML PMP samples occurring in ubiquitin pathway-mutated samples compared to samples that are wild-type for ubiquitin pathway genes. Mutations with odds ratio > 1 are likely to co-occur with ubiquitin pathway mutations, and odds ratios < 1 are likely to occur mutually exclusively with ubiquitin pathway mutations. *P* values determined by Fisher's exact test. Bars represent 95% confidence intervals.

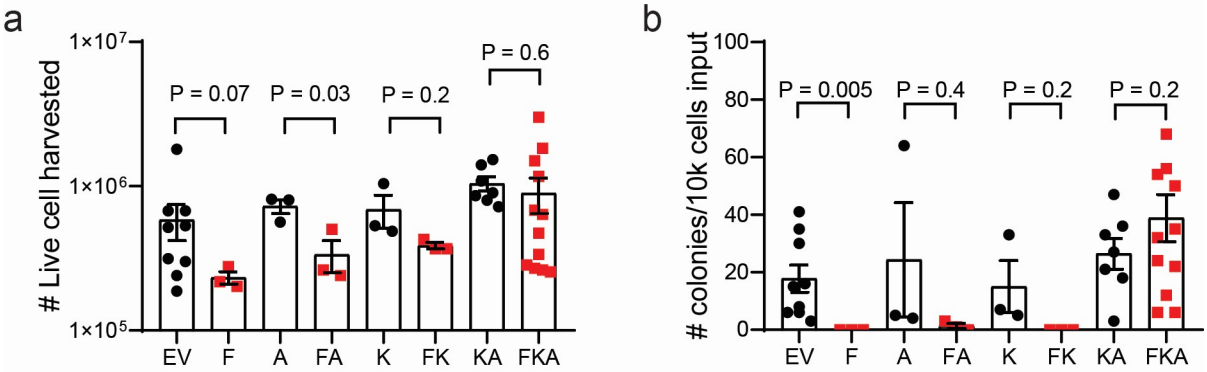

Supplementary Figure 7. Quantification of total cell numbers and CFCs in sh*FBXO11*-, *AML1-ETO*- and *KRAS*^{G12D}- transduced CD34^{+} HSPC harvested after long term culture.

a, Total live cells harvested from long-term culture were counted using trypan blue staining. **b**, CFCs were counted on day 17 after plating (*n* = 3-12 independent replicates). *P* values represent two-tailed *t*-tests and error bars represent s.d. EV = Empty vector and control shRNA; F = sh*FBXO11;* A = *AML1-ETO*; K = *KRAS*^{G12D}; FA = F + A; KA = K + A; FKA = F + K + A.

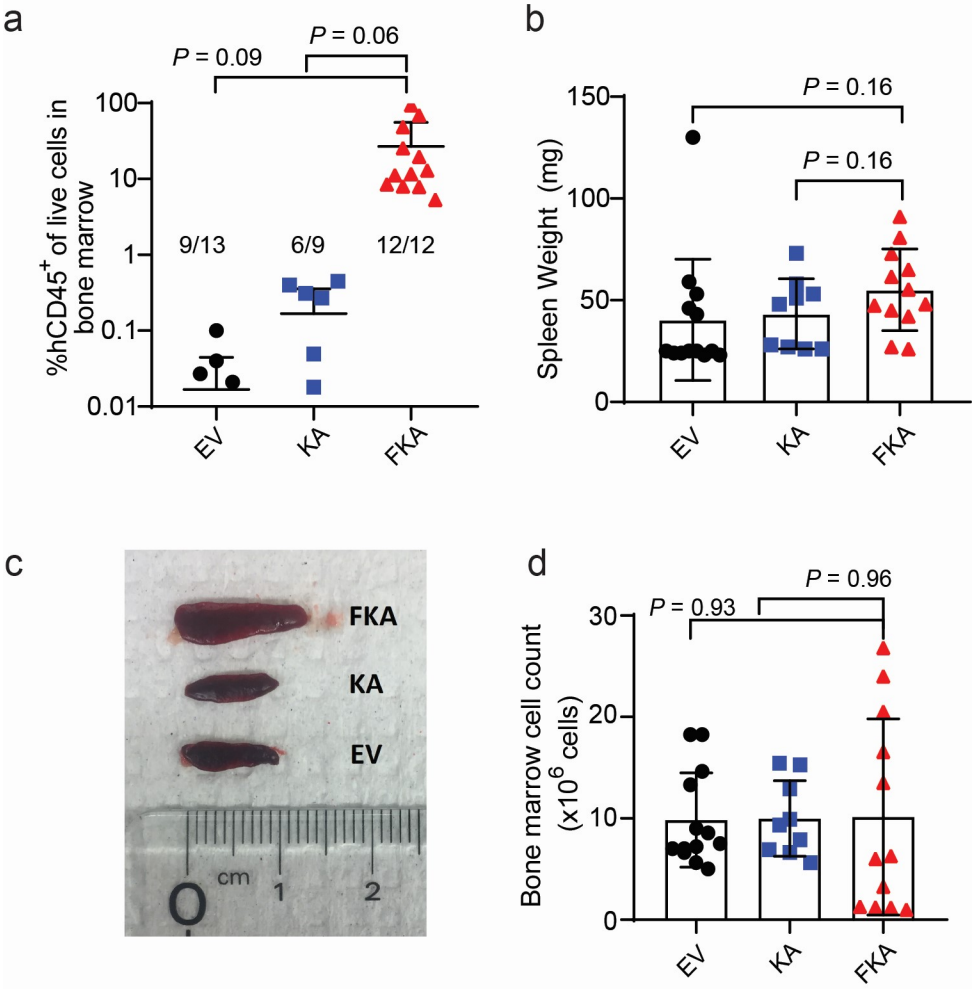

Supplementary Figure 8. Analysis of bone marrow and spleen cells from primary xenotransplanted mice at endpoint.

a, Percentages of CD34^{+}HSPC within the engrafted human hematopoietic cell population at endpoint (*n* = 5-12 mice, ND = not detected for values < 0.01%, *P* values represent Fisher's exact test). **b**, Spleen weights were measured at endpoint (*n* = 9-13 mice). **c**, Representative spleen sizes are shown. **d**, Total live cells harvested from bone marrow at endpoint were counted (*n* = 9-13 mice). *P* values represent two-tailed *t*-tests unless otherwise specified. Error bars represent s.d..

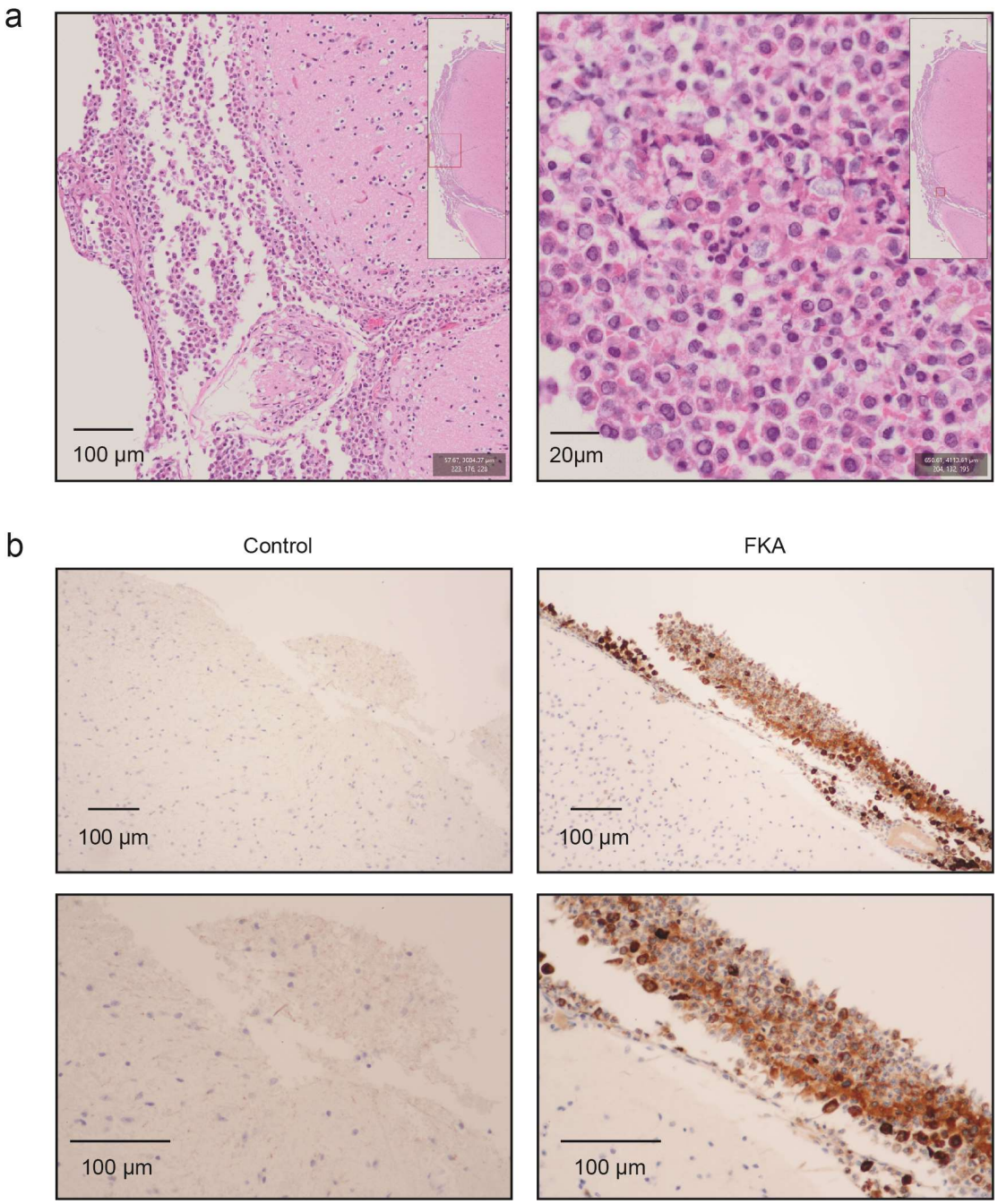

Supplementary Figure 9. Myeloid cells in the leptomeninges of FKA mice.
a, Representative hematoxylin and eosin stains performed on brain sections of FKA mice with neurologic signs at endpoint. **b**, Myeloperoxidase stains performed on brain sections of a wild-type NRG-3GS mouse and an FKA mouse, showing myeloid cell infiltration.

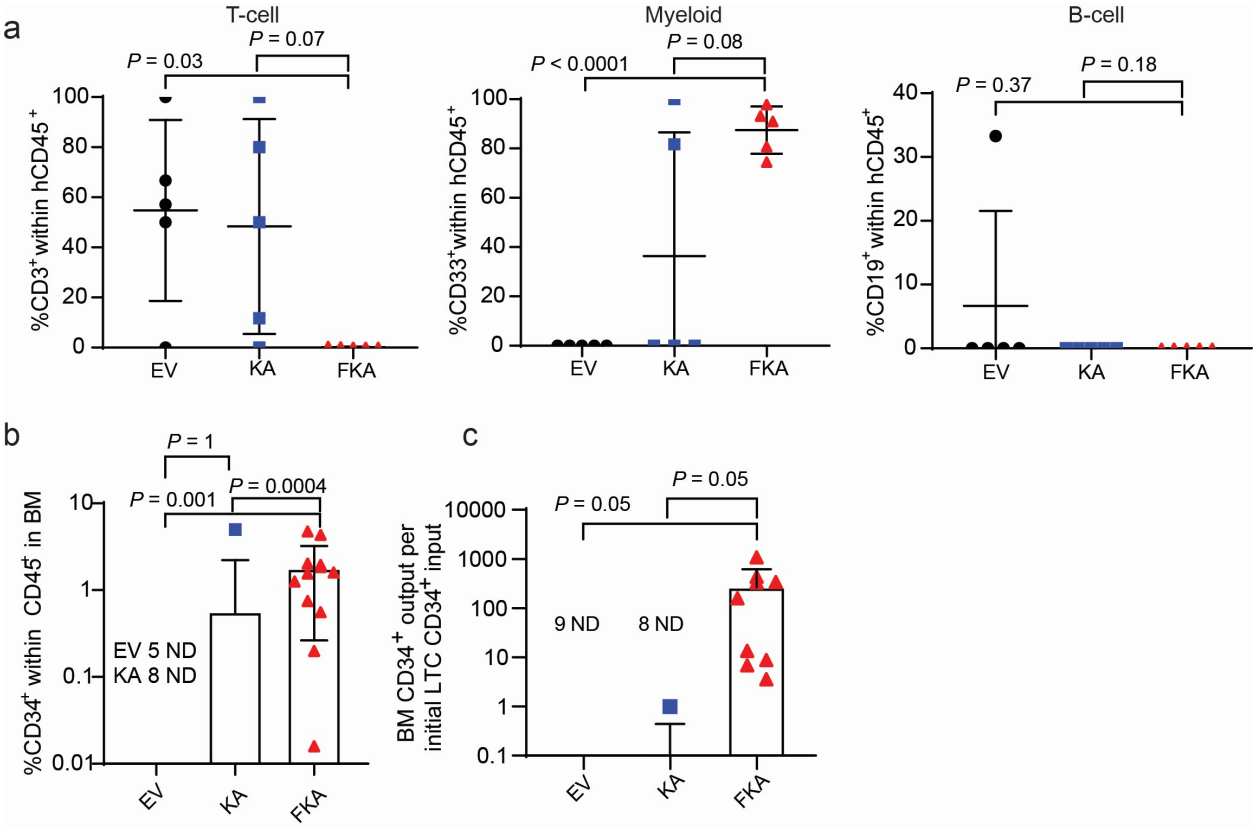

Supplementary Figure 10. Flow cytometry analysis of bone marrow cells harvested at endpoint.
a, Flow cytometry analysis of lymphoid and myeloid cell engraftment at endpoint following xenotransplantion (*n* = 5 mice). *P* values represent two-tailed *t*-tests and error bars represent s.d. **b**, Percentages of $CD34^+$HSPC within the engrafted human hematopoietic cell population at endpoint (*n* = 5-12 mice, ND = not detected for values < 0.01%, *P* values represent Fisher's exact test). **c**, Numbers of $CD34^+$ cells generated at xenotransplant endpoint per input $CD34^+$ cell seeded into long-term culture (*n* = 9 mice, *P* values represent two-tailed *t*-tests). Error bars represent s.d.

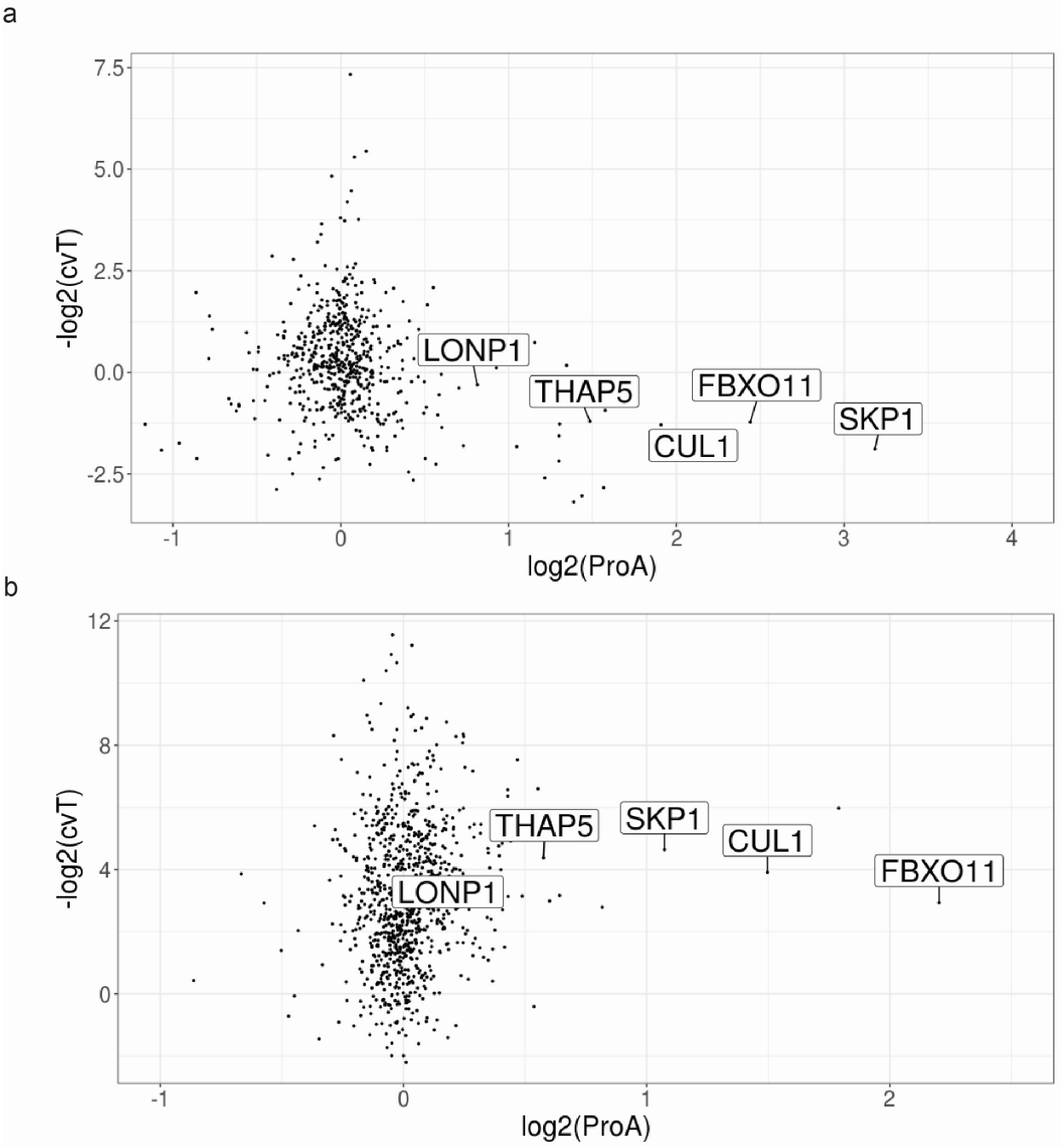

Supplementary Figure 11. Proteins co-immunoprecipitating with FLAG-FBXO11.
Mean protein abundance (log_2(ProA)) between replicates and transformed coefficient of variation (cvT) of FLAG-FBXO11 co-immunoprecipitated proteins **a**, without Benzonase® (*n* = 3 independent replicates) and **b**, with Benzonase® (*n* = 4 independent replicates), detected by quantitative tandem mass spectrometry. All detected proteins are plotted with the targets detected in both experiments labelled.

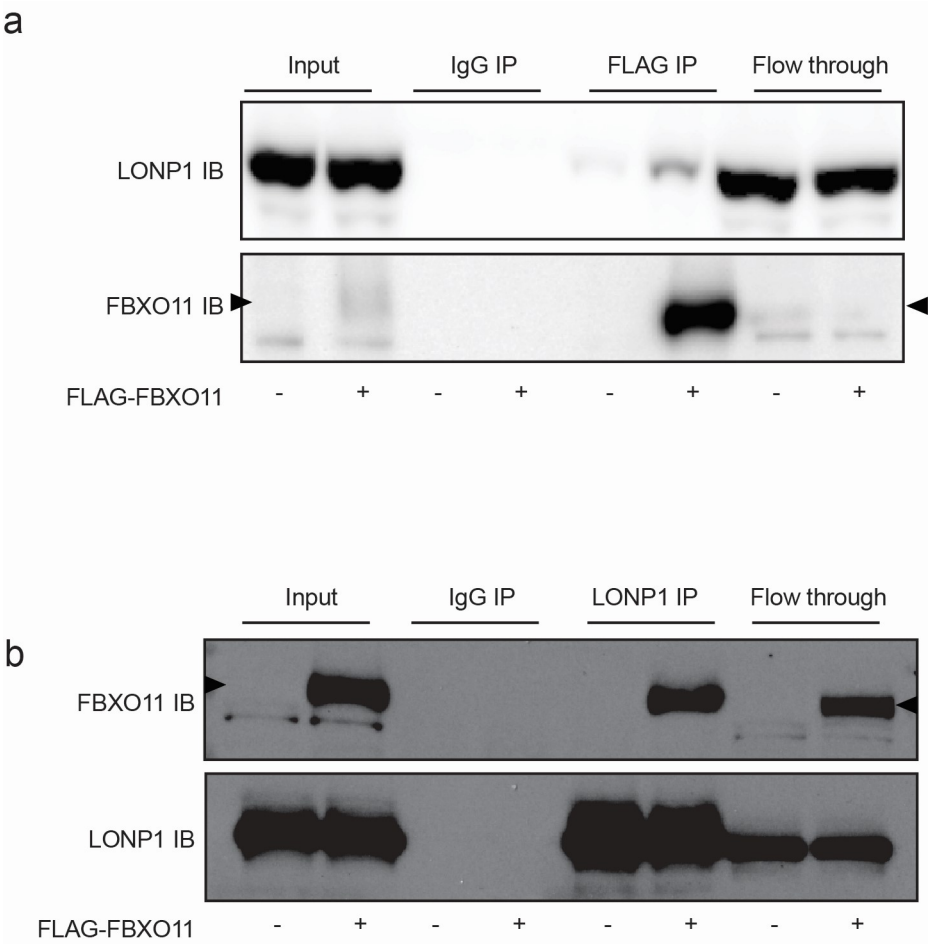

Supplementary Figure 12. LONP1 co-immunoprecipitates with FBXO11.
Co-immunoprecipitation (IP) with **a**, FLAG IP for FLAG-FBXO11 or **b**, LONP1 in *FBXO11* CRISPR KO K562 cells expressing empty vector (-) or FLAG-FBXO11 (+) followed by immunoblotting (IB) for LONP1 and FBXO11.

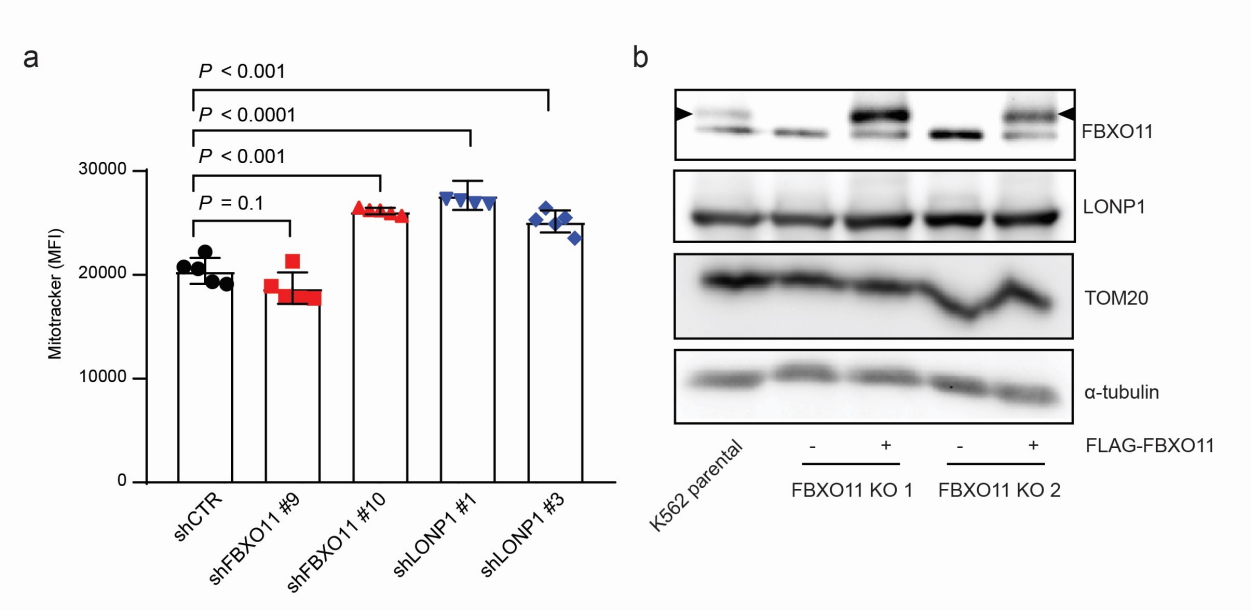

Supplementary Figure 13. Mitochondrial mass does not decrease with *FBXO11* or *LONP1* knockdown. **a**, Mitochondrial mass of CD34$^+$ HSPC expressing control shRNA or shRNA targeting *FBXO11* or *LONP1* was measured using detection of the Mitotracker dye by flow cytometry (n = 5), P values represent two-tailed t-tests and error bars represent s.d **b**, Whole cell lysates from K562 parental cells (K562) or *FBXO11* KO CRISPR clones (1-20 or 1-48) expressing empty vector (EV) or FLAG-FBXO11 (FBXO11) were immunoblotted for TOM20.

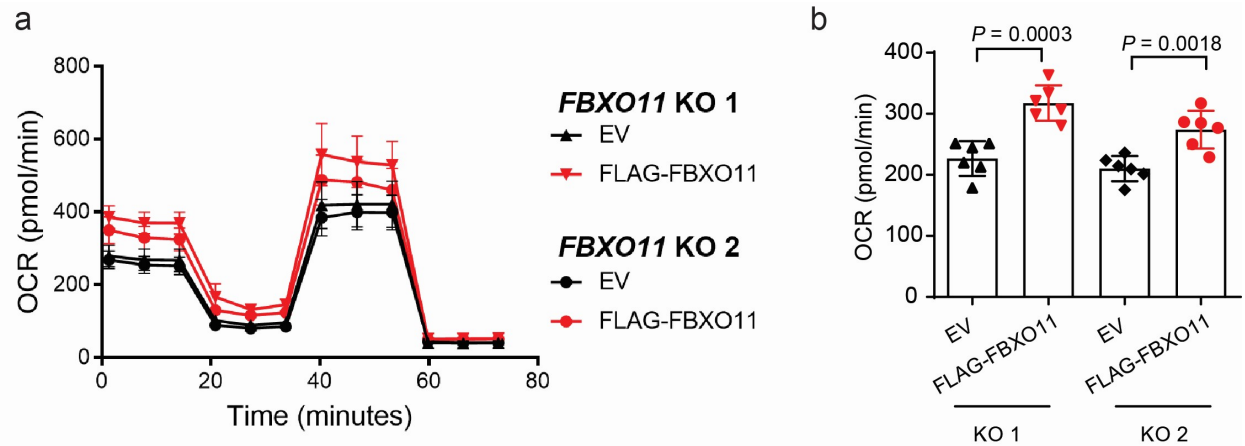

Supplementary Figure 14. *FBXO11* depletion reduces basal respiration.
a, Oxygen consumption rate (OCR) measured by the Agilent Seahorse XF Cell Mito Stress Test in K562 *FBXO11* KO cells expressing empty vector (EV) or FLAG-FBXO11. Oligomycin was added at 20 min, FCCP at 40 min, and rotenone and antimycin A at 60 min according to the manufacturer's protocol. **b**, Quantification of basal respiration in K562 *FBXO11* KO cells expressing empty vector (EV) or FLAG-FBXO11 (n = 6 independent replicates, P values represent two-tailed t-tests, error bars represent s.d.).

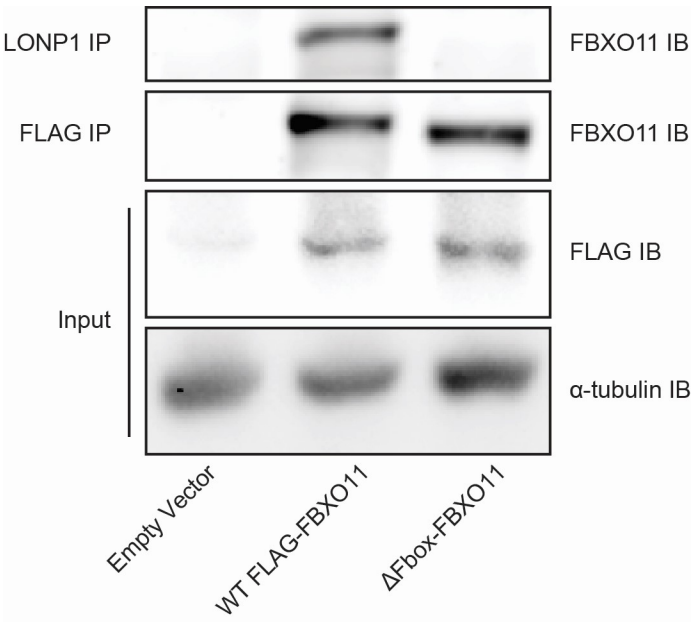

Supplementary Figure 15. ΔFbox-FBXO11 does not interact with LONP1.
Lysate from K562 *FBXO11* KO cells expressing empty vector, WT FLAG-FBXO11, or ΔFbox-FBXO11 immunoprecipitated with LONP1 or FLAG-tag antibody were immunoblotted for FBXO11.

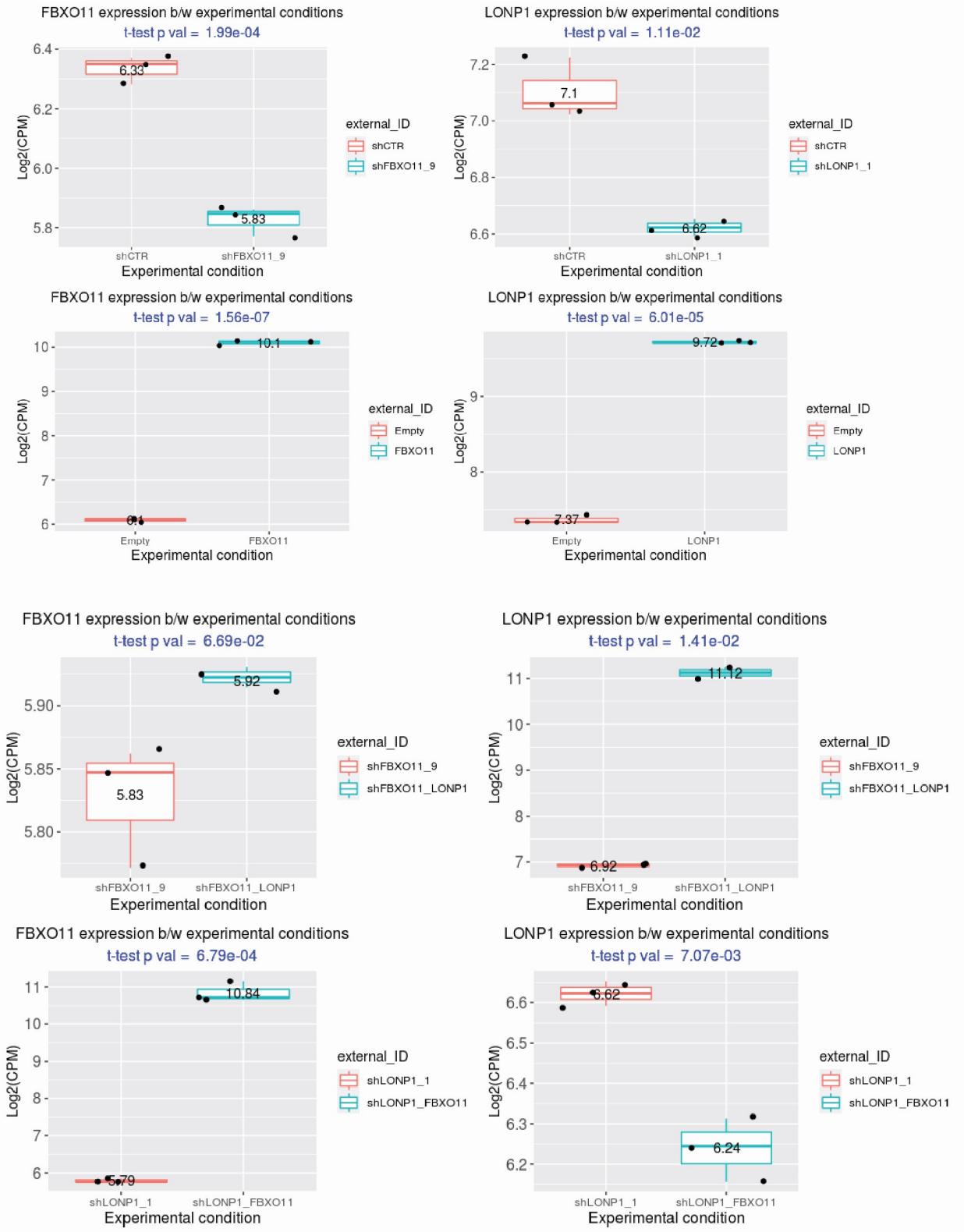
FBXO11 expression b/w experimental conditions
t-test p val = 1.99e-04
Log2(CPM)
6.33
5.83
shCTR
shFBXO11_9
Experimental condition
external_ID
shCTR
shFBXO11_9
LONP1 expression b/w experimental conditions
t-test p val = 1.11e-02
7.1
6.62
shLONP1_1
FBXO11 expression b/w experimental conditions
t-test p val = 1.56e-07
10.1
Empty
FBXO11
LONP1 expression b/w experimental conditions
t-test p val = 6.01e-05
9.72
7.37
LONP1
FBXO11 expression b/w experimental conditions
t-test p val = 6.69e-02
5.92
5.83
shFBXO11_LONP1
LONP1 expression b/w experimental conditions
t-test p val = 1.41e-02
11.12
6.92
FBXO11 expression b/w experimental conditions
t-test p val = 6.79e-04
10.84
5.79
shLONP1_1
shLONP1_FBXO11
LONP1 expression b/w experimental conditions
t-test p val = 7.07e-03
6.62
6.24

Supplementary Figure 16. Confirmation of *FBXO11* and *LONP1* transcript over-expression and/or knockdown in RNA-seq analysis.

Transcript expression of indicated genes expressed as $\log_2$(CPM) (counts per million reads mapped) between (b/w) indicated experimental conditions in CD34$^+$ HSPC RNA-seq experiment.

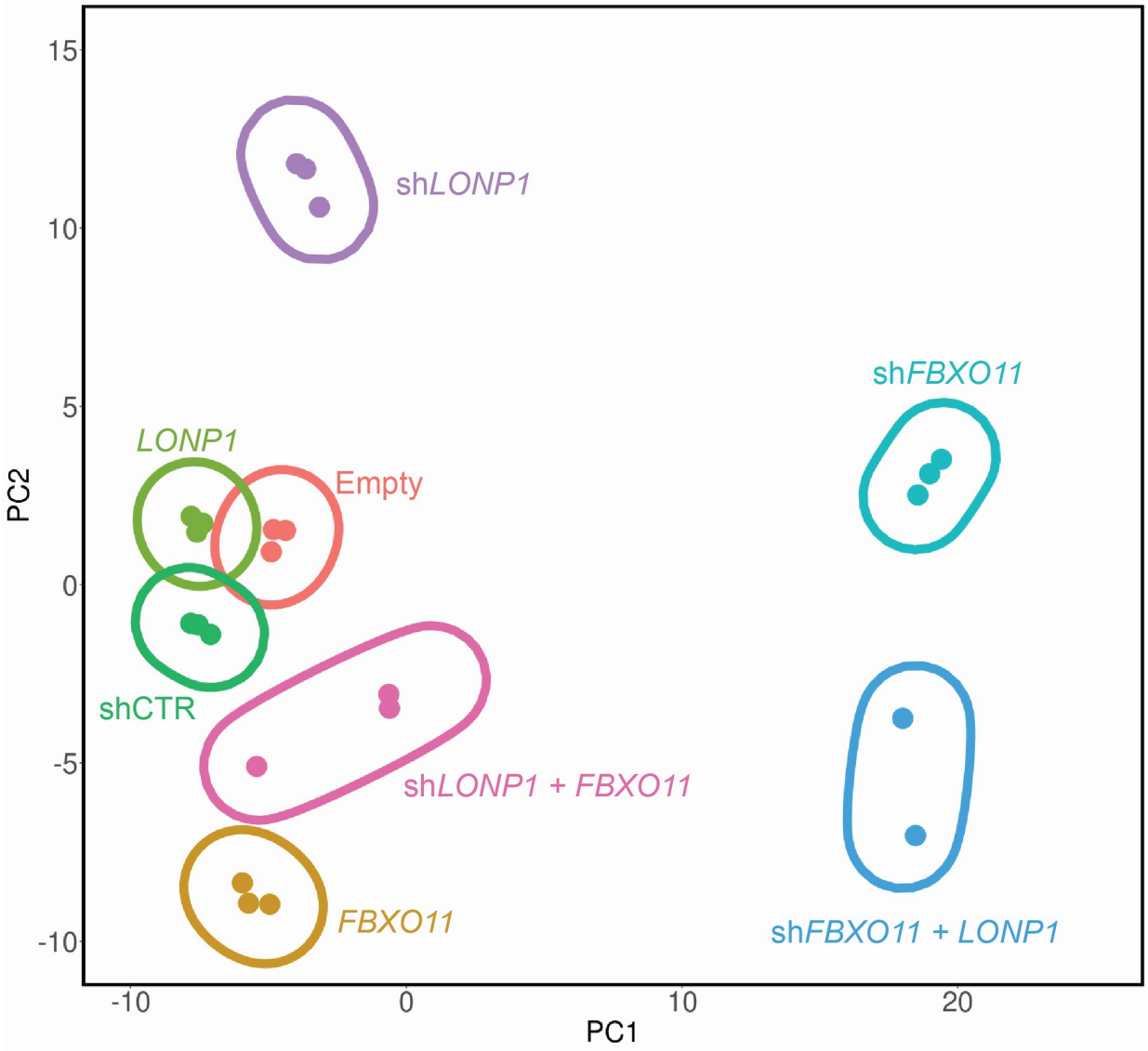

Supplementary Figure 17. Samples with enforced *LONP1* expression cluster with controls based on principal component analysis (PCA).

PCA projection of CD34$^+$ HSPC RNA-seq samples based on top 500 genes with the most variance between samples.